Master Thesis

Chair of Theoretical Solid State Physics

Arnold Sommerfeld Center for Theoretical Physics

Ludwig-Maximilians-Universität München

Effective theories of the underdoped 2D Mott Insulator

(Effektive Theorien des unterdotierten 2D-Mott-Isolators)

Shashank Anand

Supervisor:

Prof. Dr. Matthias Punk

29th June 2021

LUDWIG MAXIMILIAN UNIVERSITY

MASTER'S THESIS, 2020-2021

Effective theories of the underdoped 2D Mott Insulator

Author:
Shashank Anand

Supervisor:
Dr. Matthias Punk

A thesis submitted in partial fulfillment of the requirements for the degree of Master of Science in Physics

June 29, 2021

Acknowledgments

I would like to thank my supervisor Dr. Matthias Punk for agreeing to supervise my master's thesis. His patience and dedication towards mentoring me has instilled in me a lasting interest in theoretical condensed matter physics. The experience of working closely with him is something I will cherish for a long time to come. I am also grateful to Ludwig Maximilian University for providing an environment conducive for learning.

It is with great delight that I fondly remember the contributions of my friends and family without whose support, successful completion of this thesis is hard to imagine. My dear friends Janni, Siddharth and Koushik played an instrumental role in not only meticulously reading my thesis and giving feedback, but also in encouraging and supporting me throughout the duration of master's program. I am also greatly indebted to Kaltra, Steve and Vera for their unwavering affection and support, and for making me feel at home in Munich. I owe a debt of gratitude to my friend Keerthana for her steadfast belief in me, for her kind words of support and sympathy, and for making me realize the importance of caring for myself during stressful times. Finally, I would also like to thank my family who have provided me with everything I could possibly need to pursue my dreams.

LUDWIG MAXIMILIAN UNIVERSITY

Abstract

Effective theories of the underdoped 2D Mott Insulator

by Shashank Anand

The introduction of holes in a Mott insulator has shown to induce novel quantum states of matter in a 2D cuprate lattice which manifest at specific hole densities and temperatures. While it is clear that at large-hole densities, the system behaves as a Fermi liquid phase, the low hole-density regime characterized by a strong competition between the kinetic and interacting energies of the electrons is still not well understood.

It is seen that the Z_2 fractional Fermi liquid permeated by spinon-hole bound-state excitations has shown considerable success in explaining the features of the pseudogap metal - a phase of matter that is prominent at low doping densities. In the first part of the thesis, we use a mean-field theory of the Z_2 fractional Fermi liquid using the slave boson formalism to derive spin-spin-hole correlation functions of a Mott insulator at low doping and compare it to data seen in Quantum-gas microscopy experiments. The predictions of the model are further extended to lower temperatures where a distinctive sign-reversal of the correlation function is observed.

In the second part of the thesis, we use the slave boson picture of the t-J model to study the different phases that arise in a system which contains both free spinon and holon excitations and spinon-holon bound-state excitations. The free energy of such a system is minimized and predictions of the spinon-pairing field and the spinon-hopping field at zero temperature is obtained as a function of hole density. The results are then interpreted and possible extensions of this work are discussed.

Contents

Abstract **v**

1 Introduction **1**

2 Quantum Dimer Model **5**

3 Quantum gas microscopy experiments **9**

4 $\mathbb{Z}_2$ fractional-Fermi-liquid correlator **15**
4.1 Slave Boson description of the t-J Model 15
4.2 Electron spectral function for the $\mathbb{Z}_2$ fractional Fermi liquid 16
4.3 Evaluating correlation functions 22
4.4 Comparing with Quantum-microscopy experiments 28

5 Slave boson mean field theory with spinon/holon excitations **37**
5.1 BCS mean field theory 37
5.2 Free energy derivation 40
5.3 Phase diagram for spinon/holon excitations 42

6 Slave-boson mean-field theory with spinon-holon bound states **47**
6.1 Free energy derivation 48
6.2 Zero temperature behaviour of χ and Δ 53

7 Conclusion **57**
7.1 Outlook 59

Declaration of Authorship **65**

Chapter 1

Introduction

One of the major milestones in condensed matter theory in the latter half of the twentieth century is the successful formulation of a mathematical theory of superconductivity put forward by Bardeen, Cooper and Schrieffer, and came to be known as the BCS theory of superconductivity [1]. The paper was not only an important step closer towards our dream of achieving room temperature superconductors, it also cemented the theoretical foundations to study a whole plethora of phenomena relating to strongly correlated electron systems. However, it was soon realized that certain materials exhibited superconductivity at higher temperatures. While most metals exhibit superconductivity at $\sim$ 10K, it was seen that a certain class of cuprates exhibited superconductivity at $\sim$ 100K, an entire order of magnitude higher! A species of cuprate doped with mercury, barium and calcium, has been observed to have a record-high critical temperature of 140 K [2]. The BCS theory does not provide a mechanism to explain this phenomenon.

It soon came to be realized that cuprates played host to a multitude of other exotic phenomena that could not be understood within the scope of existing theories. The cuprates comprise of two-dimensional CuO_2 planes stacked on top of each other. Each plane consists of a square lattice with one Copper ion placed on each lattice site where each ion contains one electron in the conduction band. Despite this, the half-filled cuprate does not conduct electricity. The repulsion between electrons is so great that the motion of electrons is completely arrested. The movement of electron may, however, be restored by doppping the cuprate with holes. At large doping densities, electronic repulsion becomes small enough that the cuprates show normal metallic behaviour. A rich phase diagram of different quantum states is observed for intermediate doping densities where there is competition between the kinetic and the interaction energies of the electron. The complete phase diagram for hole doped cuprates is displayed in Figure 1.1.

Phases like the pseudogap phase and the strange metal phase have peculiar properties that have not been understood well so far [25]. However, a good starting place to understand many aspects of this system is the t-J model - a close cousin of the Hubbard model, the t-J model is attained at the limit of strong repulsive interaction between electrons [32]. In this thesis, we would like to explore the properties of the system strictly in the low hole-doping limit. In particular, we are interested in the pseudogap phase and the transitions around it.

We shall be making an important modification to the electronic operator used in the t-J model that makes it easier to study our regime of interest. Keeping in

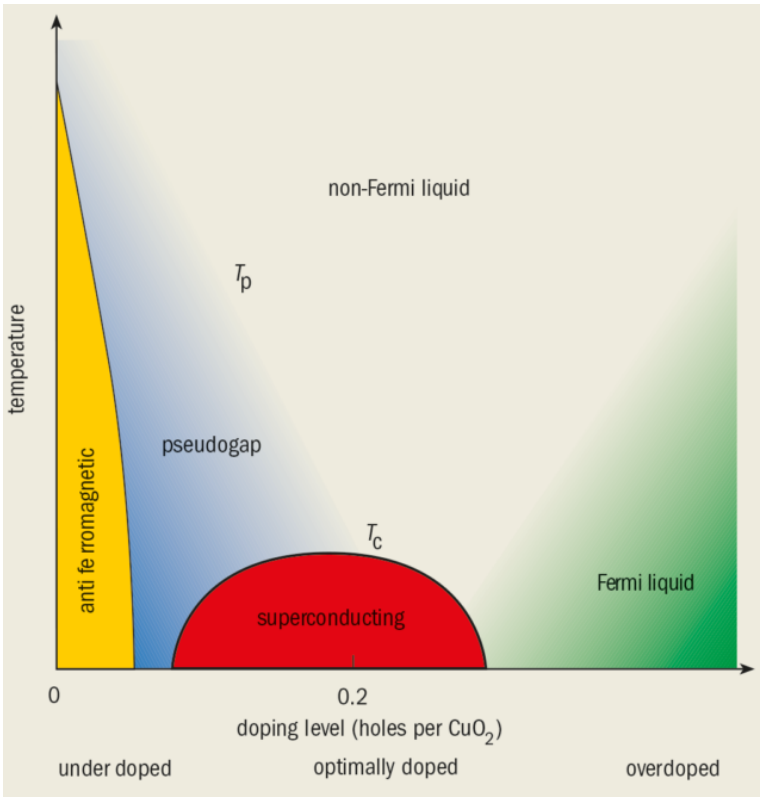

FIGURE 1.1: The phases shown here are the antiferromagnet, the pseudogap metal, the superconductor, the strange metal and the Fermi liquid. Image from [3]

mind that the half-filled lattice is treated as a lattice with no hole-doping, we write our electronic operator in a form that only counts the fluctuations about this state rather than counting a whole sea of redundant particles. By keeping track of spin and charge fluctuations below the half-filled state, this picture significantly simplifies the t-J Hamiltonian. Consider a cuprate lattice with one electron on each site and doubly occupied sites forbidden due to repulsion. Here, any given valence electron has no relative charge with respect to its environment. The only quantity of significance to our problem is its spin. In contrast, an empty lattice site introduced in the half-filled state carries a relative positive charge which needs to be tracked. Finally, there is another form of fluctuation that can traverse through the lattice and is treated as a distinct quasiparticle in this regime. It is referred to as the spinon and is characterized by the delocalization of the spin quantum number. This framework of treating the electron as a convolution of different fluctuations in the lattice was invented by Piers Coleman in the year 1983 [9] and is referred to as the slave-boson picture. It is an important concept for the purposes of our thesis and will be discussed in fair detail here.

It is often the case that one comes across two-body interaction terms in the action of strongly correlated electron systems. These terms cannot be neglected as they have a nontrivial role to play in the final predictions of the different phases of matter exhibited by the particular model. Yet, more often than not, the partition function of two-body terms cannot be evaluated, and one must resort to constructing mean-field theoretic descriptions that capture the essential features of the system by modifying the action with suitable approximations.

In our system of the underdoped Mott insulator, one conceivable approach to modify the action is to treat spinons and holons as free particles [4]. While this approach highlights many key features we expect to see in a hole-doped cuprate, it certainly has its limitations. For instance, it fails to account for at least some of the features of the pseudogap phase, namely its broken Luttinger relation and the appearance of Fermi arcs. Multiple experiments have demonstrated this in various contexts [10,11]. This thesis specifically concerns itself with the exploration of a few of the different aspects of a particular model referred to as the quantum dimer model where one assumes that the low energy excitations of the Fermi surface are permeated by spinon-holon bound states. This model is of special importance to the pseudogap phase in 2D underdoped cuprates and is discussed in Chapter 2. It has shown promise as a successful description of this phase as it is able to describe some of the key features that distinguish this phase from the others [8]. It explains the formation of Fermi-arcs which are routinely observed for this phase of matter. It also reproduces the broken Luttinger relation for the pseudogap phase. However, there are other successful models that also use a bound-state treatment of spinons and holons to describe the same phase of matter [12,13]. So, it is in our interest to look more closely at the predictions that the quantum dimer model makes. We are interested in two specific problems that give this model an opportunity to be tested.

The first problem we wish to address is that of comparing this model to the experimental data obtained by Immanuel Bloch's group. They use quantum-gas microscopy techniques on an ultracold-atom optical lattice to simulate the square-lattice Hubbard model and measure lattice correlations around an introduced dopant as a function of distance and hole density. [6,7]. The details of this experiment are discussed in Chapter 3. Quantum-gas microscopy has enabled the direct, real-space characterization of strongly correlated electron systems. In cold-atom lattice simulators [33], this technique has allowed tests to be performed on the Fermi-Hubbard model which includes the detection of long-range spin correlations [34], charge and spin-transport in two dimensions [35,36], as well as incommensurate magnetism in one dimension[37]. In the experiments described here, this technique is utilized by Bloch's group to characterize the nature of electronic correlations that arise around a dopant. These experiments are performed at a temperature scale of $T \sim 1.4J$ where J is the antiferromagnetic coupling observed at half-filling. In cuprates, this quantity is estimated at $J \sim 100meV \sim 1100K$. Since no existing model successfully explains Bloch's data at low doping densities, this is a good opportunity to use the dimer model to obtain these correlation functions and compare them with these experiments. We calculate an effective mean-field Hamiltonian of the $\mathbb{Z}_2$ fractional Fermi liquid. USing this, spin-spin-hole correlators are evaluated and compared to the quantum-gas microscopy experiments. This is discussed in Chapter 4.

The next problem we explore involves predicting the phases that arise when one writes out the t-J action with spinon-hole bound-state excitations and free spinon-holon fluctuations. First, we follow the discussion in Kotliar and LIu [4] to understand the different phases of matter that arise in a system with only spinon/holon fluctuations. This is discussed in Chapter 5. Next, we follow a similar procedure to obtain the phase diagram of a system with both kinds of fluctuations in Chapter 6. The free energy of such a system is obtained by integrating out all the fermionic degrees of freedom in the problem. The resulting free energy is then minimized with respect to the different order parameters in the problem. Thus, at different temperatures and hole densities, we find that different phases manifest when the free energy is minimized. In this thesis, due to time constraints, we only study the zero temperature behaviour of the order parameters. Finally, we discuss possible implications of our results and conceivable extensions of our work in Chapter 7.

Chapter 2

Quantum Dimer Model

Soon after the discovery of cuprates, it was realized that there was a distinct quantum phase of matter that sets in at low doping densities and that this phase of matter was robust even at temperatures significantly higher than the critical temperature of the superconducting phase. This phase of matter came to be known as the pseudogap metal. The pseudogap metal has two important features that serve to distinguish it from the other phases. Firstly, they appear to violate Luttinger's relation (which states that the area of the Fermi surface must be proportional to the charge-carrier density in the conduction band). In cuprates, it is conventional to define the hole density with reference to the Mott-insulating state at half filling. So, with respect to a fully filled lattice where each lattice site has two electrons of opposite spins, the hole density in the system is $1+\delta$ (where δ is the density of hole-dopants introduced beyond half-filling). Thus, following Luttinger's relation, we expect that the area of the Fermi surface grows as $1+\delta$. This is, in fact, seen at high percentages of doping. However, at low δ, it is seen that the system behaves as a Fermi liquid with a Fermi surface whose area is proportional to δ. Secondly, a curious feature of the pseudogap metal is that experiments have consistently shown the presence of gaps in the Fermi surface [17,18,19]. This seemingly broken surface came to be known as Fermi arcs. These arcs appear around the nodal points $(\pm\pi/2, \pm\pi/2)$ on the Brillouin zone. They are presented in Figure 2.1.

An early study [4] proposed that the pseudogap phase can be characterized by a doped Mott insulator that undergoes spin-charge separation. However, this can never account for the broken Fermi surface as a convolution of free spinons and holon-spectral functions always posses a smooth closed Fermi surface and cannot produce a sharp Fermi surface. Despite the broken Fermi surface, there is good reason to suppose that these are metals as they appear to obey Fermi liquid theory. Firstly, optical conductivity experiments [14] reveal that the quasiparticle lifetime of this phase of matter displays a dependence identical to that of the Fermi liquid $1/\tau \propto ((\hbar\omega)^2 + (c\pi k_B T)^2)$with c an order unity constant. Also, the in-plane magnetoresistance of the pseudogap is proportional to $\tau^{-1}(1+bH^2\tau^2+...)$ where $\tau \sim T^{-2}$ and b is a T-independent constant and H is the applied magnetic field. This is true for Fermi liquids as well. In fact, this is Kohler's rule for a Fermi liquid [15].

A simple model of a fractional Fermi liquid which is referred to as the quantum dimer model, was developed in [8]. The Hilbert space of the dimer model is spanned by two species of dimers. The first is a boson with no spin and charge relative to the Mott insulator at half-filling. The second is a fermion with both spin and charge $+e$.

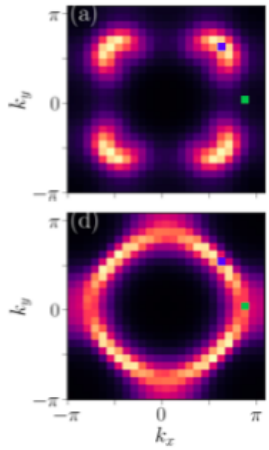

FIGURE 2.1: The top image depicts the Fermi arcs while the bottom image depicts a complete Fermi surface for a Fermi liquid. The blue dots in both images represents a nodal point $(\pi/2, \pi/2)$ whereas the green dots represent an antinodal point $(\pi, 0)$. Figure from [16].

These dimers satisfy the 'hard-core' constraint which states that no two dimers can overlap with each other. (From this, it follows, for instance, that you cannot have a hole entangled simultaneously with two electrons that are on one lattice site.) They are represented in terms of electron operators in the following manner:

$$D^{\dagger}_{i,\eta} = \frac{\gamma_{i\eta}}{\sqrt{2}}(c^{\dagger}_{i,\uparrow}c^{\dagger}_{i+\eta,\downarrow} + c^{\dagger}_{i+\eta,\uparrow}c^{\dagger}_{i,\downarrow})|0\rangle, \quad F^{\dagger}_{i,\eta\alpha} = \frac{\gamma_{i\eta}}{\sqrt{2}}(c^{\dagger}_{i,\alpha} + c^{\dagger}_{i+\eta,\alpha})|0\rangle, \tag{2.1}$$

where $\gamma_{i\eta}$ is a phase factor that can be suitably adjusted. The first term is a spin singlet containing two electrons of opposite spins mutually entangled with each other and is chargeless relative to the half-filled state. In contrast, the fermion defined on the right of equation 2.1 represents a bound state formed between a hole and an electron from their short-range mutual attraction.

The picture in Figure 2.2 suggests that the dimers live on the bonds between lattice sites as one can associate a characteristic directional orientation for particles that arises from these bonds. They impart a nontrivial exponential factor when we write the creation operator of the electron-hole bound states in momentum space. This term plays a central role in the success of this model in explaining all the unique features of the pseudogap metal.

We present the quantum-dimer Hamiltonian that acts on the Hilbert space described containing the bosonic and fermionic dimers discussed above. A detailed discussion on motivating this Hamiltonian can be found in [8]. The Hamiltonian is written as a sum of two parts. The first part is the Rokhsar Kivelson Hamiltonian [38] $\mathcal{H}_{RK}$ that describes hopping and interactions of the bosonic dimers alone. The second part, represented by the Hamiltonian $\mathcal{H}_1$ characterizes the interaction between bosonic and fermionic dimers and contains single fermionic hopping terms. Slightly

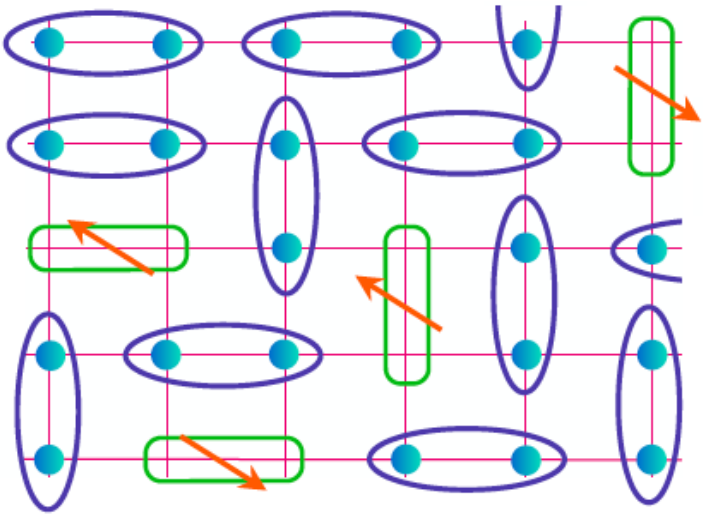

FIGURE 2.2: The figure shows a pictorial representation of electrons on a square lattice below half filling arranged in a $\mathbb{Z}_2$ fractional Fermi liquid formation. The quasiparticles with spins are electron-hole bound states whereas the other quasiparticles are two-electron bound states. Figure from [8].

below half-filling, the number of fermionic dimers is low enough to ignore two-body fermionic interaction and so, such interactions are neglected here. The Hamiltonian is given by:

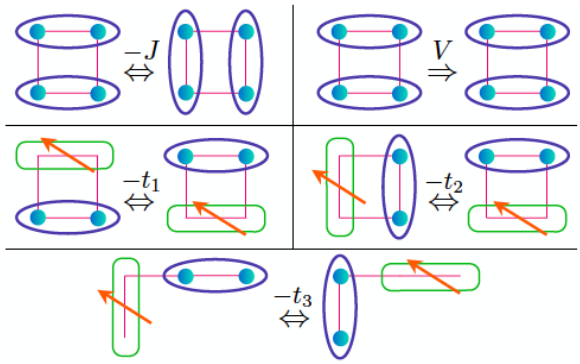

FIGURE 2.3: Interactions coupled by J and V come from dimer hopping. The parameters that couple with t_1, t_2 and t_3 describe single fermionic hopping. Image from [8].

$$
\begin{aligned}
\mathcal{H} &= \mathcal{H}_{RK} + \mathcal{H}_1, \\
\mathcal{H}_{RK} &= \sum_i \Big[-J D^\dagger_{ix} D^\dagger_{i+\hat{y},x} D_{iy} D_{i+\hat{x},y} + 1 \text{ term} , \\
&\quad + V D^\dagger_{ix} D^\dagger_{i+\hat{y},x} D_{ix} D_{i+\hat{y},x} + 1 \text{ term} \Big] \\
\mathcal{H}_1 &= \sum_i \Big[-t_1 D^\dagger_{ix} F^\dagger_{i+\hat{y},x\alpha} F_{ix\alpha} D_{i+\hat{y},x} + 3 \text{ terms} \; - t_2 D^\dagger_{i+\hat{x},y} F^\dagger_{iy\alpha} F_{ix\alpha} D_{i+\hat{y},x} + 7 \text{ terms} \\
&\quad - t_3 D^\dagger_{i+\hat{x}+\hat{y},x} F^\dagger_{iy\alpha} F_{i+\hat{x}+\hat{y},x\alpha} D_{iy} + 7 \text{ terms} \; - t_3 D^\dagger_{i+2\hat{y},x} F^\dagger_{iy\alpha} F_{i+2\hat{y},x\alpha} D_{iy} + 7 \text{ terms} \Big],
\end{aligned}
\tag{2.2}
$$

where the terms that are not displayed are generated by symmetry operations that are valid for the square lattice. The specific operations of each term in the Hamiltonian can be understood by looking at Figure 2.3. This model is used to construct an effective tight-binding Hamiltonian for the $\mathbb{Z}_2$ fractional Fermi liquid ($\mathbb{Z}_2\ FL^*$, which will be discussed in subsequent sections. We aim to compare the $\mathbb{Z}_2$ fractional Fermi liquid with experiments performed on the underdoped Mott insulator using quantum-gas microscopy techniques. In the next chapter, we shall discuss in detail the results obtained in the quantum-gas microscopy experiments. It is seen here that a magnetic polaron forms around a given dopant at low doping densities. It is hoped that the $\mathbb{Z}_2$ fractional Fermi liquid also reproduces the same correlation structures as well.

Chapter 3

Quantum gas microscopy experiments

Polarons are charge carriers that are wrapped by a local polarization that distinguishes them from their background environment. They are among the most fundamental quasiparticles in interacting many-body systems and emerge even at the level of a single dopant. A series of experiments [7] performed by Immanuel Bloch's group demystified the real-space structure of magnetic polarons that can form when a Mott insulator is doped with a small population of holes. In the phase diagram for cuprates in Figure 1.1, we see that hole doping can take the system from the antiferromagnetic regime to the pseudogap regime if the temperature is high enough. The antiferromagnetic correlations between the valence electrons on the lattice sites are disrupted with the introduction of holes. We see in Figure 3.1 that polarons are indeed formed around the doped sites as the correlations switch their sign abruptly as one moves away from the dopant. This is a signature of the magnetic polaron. Bloch's group successfully managed to obtain a real-space image of this quasiparticle.

Consider the following correlation function:

$$C(r_0; r, d) := 4 \left\langle S^z_{r_0+r-d/2} S^z_{r_0+r+d/2} \right\rangle_{:r_0, r_0+r-d/2, r_0+r+d/2}. \tag{3.1}$$

The above 3-point correlation is interesting to us as this can be employed to quantify the nature of correlations between electrons in the presence of dopants. Here, $d = |r_2 - r_1|$, $r = \dfrac{|r_1 + r_2|}{2}$ and r_0 is the position of the dopant, r_1 and r_2 refer to the positions of electrons between which the correlation is calculated.

In this setup in Figure 3.1, we see a lattice with one valence electron on each lattice site. At the origin , we have a dopant that gives rise to a doublon which is a quasiparticle with two electrons having opposite spins residing on the same lattice site. Strictly speaking, electron doping is not equivalent to hole doping as the phases observed for the overdoped and underdoped Mott-insulator are structurally different. However, it is seen that for systems which only allow nearest neighbour hopping, particle-hole asymmetry completely disappears and the overdoped and underdoped Mott insulator have identical phases. [25,27]. An optical lattice with cold atoms

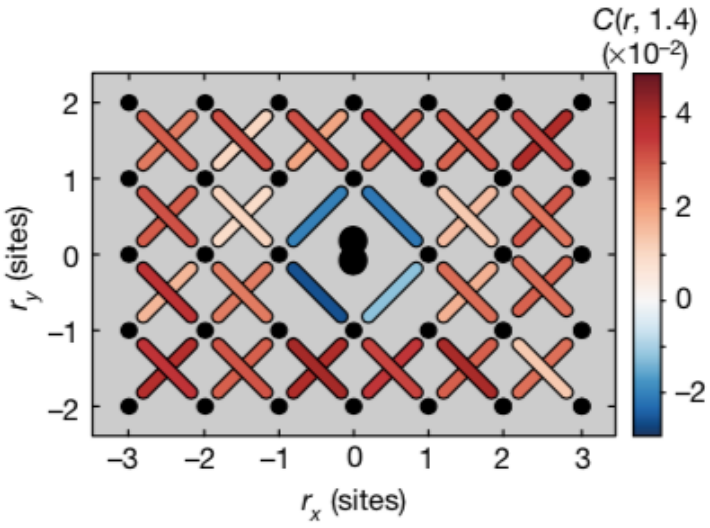

FIGURE 3.1: Figure shows the different correlations that were measured with respect to the doublon site displayed in black. The red bonds are positive diagonal correlation whereas the blue line signifies a negative diagonal correlation. Figure from 7

is such a system as the next-to-nearest-neighbour hopping amplitude is almost non-existent. Thus, what is observed in Figure 3.1 is equally applicable if the dopant were a hole instead.

It is seen from Figure 3.1 that the nearest neighbour electrons around the dopant correlate with each other negatively while all other diagonal correlations are positive. There is an abrupt sign reversal observed when one measures diagonal correlations with the innermost electrons and contrasts it with diagonal correlations elsewhere on the lattice. It is seen in Figure 3.1 that the central bubble inside is reminiscent of a polaron, as the doublon reverses the sign of the correlations of the electrons around it thereby distorting the antiferromagnetic correlations of the Mott-insulating phase. But the doublon and the cloud of sign-reversed correlations may be thought of as a single unit moving through a sea of antiferromagnetic bonds. This single unit is the magnetic polaron.

We see from the phase diagram of 2D cuprates that hole-doping allows the system to transition out of the antiferromagnetic regime into a new phase of matter that is distinct from the Fermi liquid. Our current understanding of cuprates does not allow us to predict the doping densities and temperatures at which this transition happens, but we recognize that one possible state is the pseudogap metal. Since the dimer model has shown to be a simple yet effective description of the pseudogap metal [8], one ought to check if the dimer model shows any success when one compares its prediction of the spin-spin-hole correlator at the appropriate hole-density and temperature, to the data obtained by Bloch's group. Here the spin-spin-hole correlator works just like a spin-spin-doublon correlator as this system is expected to uphold particle-hole symmetry.

In the phase diagram of 2D cuprates below half-filling seen in Figure 1.1, the system begins at the Mott-insulating state at half filling (zero doping) and ultimately reaches the Fermi liquid regime at high doping densities. As it does this, it encounters phases that are dominated by non-Fermi interactions. The transition of a system through different phases can be realized through experiment by measuring the electronic correlations around dopants as a function of hole density. Performing these measurements at increasing levels of hole-doping allows us to infer the different regimes which manifest. So, this is a strong motivation to experimentally study spin-spin-hole correlators for 2D cuprates as a function of hole density, as was done in [6].

When the system is in the antiferromagnetic regime, the correlations between nearest neighbour electrons are strictly negative, while diagonal correlations are positive. In the Fermi-liquid regime which is seen at high doping densities, we may employ a tight-binding model for electrons with no other interaction terms to calculate the required correlations. It is seen that in this regime, Pauli exclusion principle disfavours the presence of multiple electrons of the same spin close to each other. So a negative correlation between nearest neighbours is observed. For non-Fermi liquids that manifest at intermediate doping densities, we are still in need of a theoretical model that explains the electronic correlations seen here.

This sets the stage to test various interacting toy-models to explain phases seen at intermediate doping regimes. The $\mathbb{Z}_2$ fractional Fermi liquid has shown reasonable success at describing the pseudogap phase [8,24]. If the pseudogap phase is indeed an intermediate phase through which the system traverses, then it is reasonable to suppose that this model holds potential to explain the correlations in the appropriate hole density range.

First, the two-point connected-correlation function is measured for different configurations. The fact that it is connected helps us filter out background signals that come from the non-interacting terms in the correlation function. The two-point correlation function for this system is given by:

$$C^{(c)}(d) = C^{(c)}(r_1, r_2) = \eta \left(\langle \hat{S}_{r_1} \hat{S}_{r_2} \rangle - \langle \hat{S}_{r_1} \rangle \langle \hat{S}_{r_2} \rangle \right), \tag{3.2}$$

where $\eta = 1/(\sigma(\hat{S}_{r_1})\sigma(\hat{S}_{r_2}))$ is the normalization, r_1, r_2 represent the positions of the electrons between which we are measuring the correlations.

As shown in Figure 3.2, for different configurations, we see a sign reversal of the curve somewhere at $\delta \sim 20\% - 40\%$ hole doping density. At low doping densities, the hole perturbs all the bonds in its vicinity such that the nearest neighbours have a positive correlation with each other and the next to nearest neighbours are negatively correlated. They are reminiscent of magnetic polarons moving through the system with an antiferromagnetic environment. A given hole and all the electrons immediately surrounding it constitute a polaron. At $\delta \sim 20\%$, there is one hole for every four electrons. This suggests that neighbouring polarons overlap to such an extent

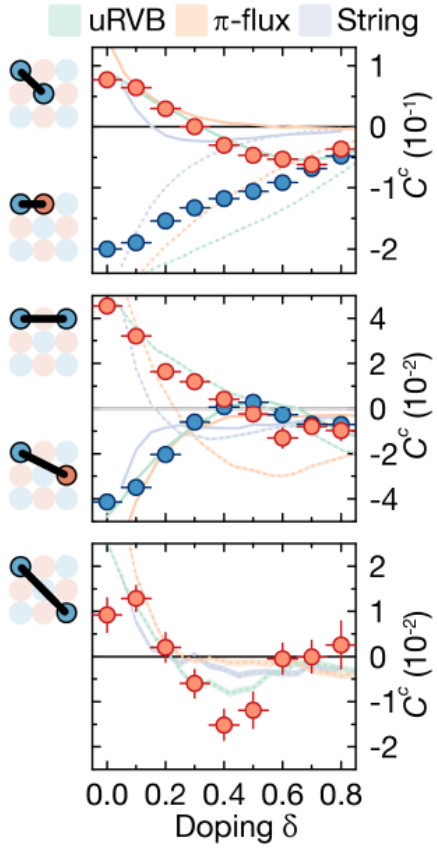

FIGURE 3.2: shows the different configurations for which correlations were measured, the graphs display the corresponding correlation function as a function of hole density. Furthermore,the predictions of theoretical models that includes the uniform RVB phase, the π flux model and the string model (as mentioned in the legend) have all been plotted along with the data to compare with the data points. Figure from [6].

that all bonds throughout the lattice are uncorrelated as they belong to two different polarons at the same time. This scaling argument is confirmed in Figure 3.2 as the curve crosses the x-axis at roughly this doping density. At high percentages of doping, it is important to take Pauli's exclusion principle into account, as they disfavour fermions of the same spin from occupying a small area, and so, one expects weak negative correlations between all lattice sites at higher doping densities.

While looking at the two-point correlation function is certainly instructive, our main quantity of interest is the spin-spin-hole three-point correlation. This quantity is important because it describes how the dopant affects two-point correlation functions at different distances. This also provides a good testing ground for different theories as different toy models tend to differ in their predictions of this function. This is apparent in Figure 3.3 where it is seen that the predictions made by different theories deviate significantly from each other.

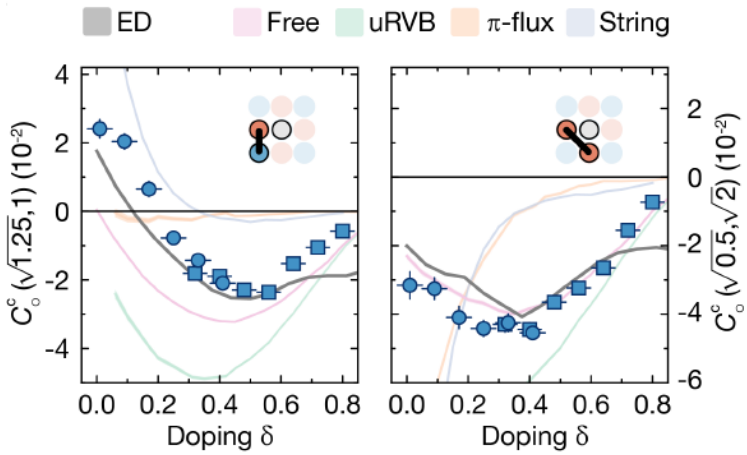

FIGURE 3.3: Figure shows the two configurations for which the correlations are plotted against hole density δ. Predictions of the theories mentioned in the legend are also plotted along with the data points. Figure from [6].

The three-point correlation function looks like the following:

$$\begin{aligned} C^c_0(r,d) =& C^c_0(r_3;r_1,r_2) = \eta C^c_3(r_3;r_1,r_2), \\ =& \eta(\langle \hat{h}_3 \hat{S}^{\mathbb{Z}}_2 \hat{S}^z_1 \rangle - \langle \hat{h}_3 \rangle \langle \hat{S}^{\mathbb{Z}}_2 \hat{S}^z_1 \rangle - \langle \hat{S}^{\mathbb{Z}}_2 \rangle \langle \hat{h}_3 \hat{S}^z_1 \rangle \\ & - \langle \hat{S}^z_1 \rangle \langle \hat{h}_3 \hat{S}^{\mathbb{Z}}_2 \rangle + \langle \hat{h}_3 \rangle \langle \hat{S}^{\mathbb{Z}}_2 \rangle \langle \hat{S}^z_1 \rangle). \end{aligned} \tag{3.3}$$

For spin-balanced systems (i.e. $\langle S^z \rangle = 0$):

$$C^c_0(r,d) = \eta(\langle \hat{h}_3 \hat{S}^{\mathbb{Z}}_2 \hat{S}^z_1 \rangle - \langle \hat{h}_3 \rangle \langle \hat{S}^{\mathbb{Z}}_2 \hat{S}^z_1 \rangle), \tag{3.4}$$

where r is the length of the bond between the fermions, d is the distance of the bond from the dopant under consideration, and η is the normalization factor given by [6]:

$$\eta = 1/\left(\langle \hat{h}_3 \rangle \sigma(\hat{S}_2^{\mathbb{Z}}) \sigma(\hat{S}_1^z)\right). \tag{3.5}$$

An important feature of this graph is that the diagonal correlations are always negative, but for nearest neighbour correlations, there is a crossover at around $\delta \sim 20\%$. In the left hand side graph of figure 3.3, we see that most existing theories do reasonably at higher doping but fail to at low hole densities. Other than performing a rigorous exact diagonalization of the t-J model, which is cumbersome, there exists no approximate theory that predicts the crossover that is seen here. This allows us to test the $\mathbb{Z}_2$ fractional Fermi liquid, which is described in the next chapter.

Chapter 4

$\mathbb{Z}_2$ fractional-Fermi-liquid correlator

4.1 Slave Boson description of the t-J Model

The t-J model, which is the strong-interaction limit of the Hubbard model, is believed to offer accurate insights into the workings of cuprates [25]. So, we shall turn our attention to this model in order to understand the emergence of the pseudogap phase. To do this, we start off with the t-J model and introduce spinon-hole bound state operators through a Hubbard Stratonovich (H.S.) transformation. Once that is done, we construct a tight-binding Hamiltonian that describes the hopping of the bound-state particles. This is equivalent to finding an effective free particle description of spinon-hole bound states which comes in handy as we evaluate expectation values and correlation functions later. But, in order to build this Hamiltonian from the t-J model, we resort to writing a Ginzburg-Landau free energy description of the low energy excitations of the system and understand the role of each coupling term in enabling different dimer hopping modes to persist. Finally, we make use of this Hamiltonian to obtain an electronic spectral function that provides a bridge between the quantum dimer model and measurable quantities like electronic correlation functions and the electronic momentum distribution. This enables us to derive spin-spin-hole correlations and compare the predictions of the quantum dimer model with data that is obtained by Bloch's group. We start this process by stating the Hamiltonian in the t-J model [28].

$$\mathcal{H} = \sum_{\langle ij \rangle} J(S_i.S_j - \frac{1}{4}n_i n_j) - \sum_{ij,\sigma} t_{ij}(c^{\dagger}_{i\sigma}c_{j\sigma} + h.c.), \tag{4.1}$$

where $t_{ij} = t, t', t''$ for the nearest, second nearest, and third nearest neighbour-pairs respectively. We have the additional constraint that double occupation is forbidden. This constraint is hard to impose in practise. So, we use the slave boson description of the electron as this incorporates this constraint into the operators itself. The electronic creation operator can thus be broken down into fluctuations about the half-filled Mott insulator and is represented by [25]:

$$c^{\dagger}_{i\sigma} = f^{\dagger}_{i\sigma}b_i + \epsilon_{\sigma\sigma'}f_{i\sigma'}d^{\dagger}_i, \tag{4.2}$$

where $f^\dagger_{i\sigma}$ is the spinon creation operator, b_i is the holon term and $d^\dagger_i$ is the doublon creation operator. But we want to exclude double occupancy as it constitutes a higher order effect and we are only interested in the low energy excitations of the t-J model. Thus, we are finally left with:

$$\begin{aligned} c^\dagger_{i\sigma} &= f^\dagger_{i\sigma} b_i, \\ f^\dagger_{i\uparrow} f_{i\uparrow} + f^\dagger_{i\downarrow} f_{i\downarrow} + b^\dagger_i b_i &= 1. \end{aligned} \tag{4.3}$$

Using the spin representation as given in [29]:

$$S_i.S_j = -\frac{1}{4} f^\dagger_{i\alpha} f_{j\alpha} f^\dagger_{j\beta} f_{i\beta} - \frac{1}{4}(f^\dagger_{i\uparrow} f^\dagger_{j\downarrow} - f^\dagger_{i\downarrow} f^\dagger_{j\uparrow})(f_{j\downarrow} f_{i\uparrow} - f_{j\uparrow} f_{i\downarrow}) + \frac{1}{4} f^\dagger_{i\alpha} f_{j\alpha}. \tag{4.4}$$

Finally, we write

$$\begin{aligned} n_i n_j =& (1 - b^\dagger_i b_i)(1 - b^\dagger_j b_j), \\ \approx& 1 - b^\dagger_i b_i - b^\dagger_j b_j. \end{aligned} \tag{4.5}$$

Plugging equations 4.3, 4.4 into 4.1 in the Hamiltonian [25] then gives:

$$\begin{aligned} \mathcal{H} = \sum_{\langle ij \rangle} \Big[J \big[&- \frac{1}{4} f^\dagger_{i\alpha} f_{j\alpha} f^\dagger_{j\beta} f_{i\beta} - \frac{1}{4}(f^\dagger_{i\uparrow} f^\dagger_{j\downarrow} - f^\dagger_{i\downarrow} f^\dagger_{j\uparrow})(f_{j\downarrow} f_{i\uparrow} - f_{j\uparrow} f_{i\downarrow}) + \frac{1}{4} f^\dagger_{i\alpha} f_{j\alpha} \big] \\ &- \frac{1}{4}(1 - b^\dagger_i b_i)(1 - \bar{b}_j b_j) \Big] - t \sum_{ij\sigma} (f^\dagger_{i\sigma} b_i b^\dagger_j f_{j\sigma} + h.c.). \end{aligned} \tag{4.6}$$

4.2 Electron spectral function for the $\mathbb{Z}_2$ fractional Fermi liquid

In many-body physics, one often encounters quartic terms whenever there is a non-trivial two-body interaction term involved in the Hamiltonian. The expectation values of these quartic terms are hard to evaluate exactly. But the H.S. transformation is a systematic framework in which one can reduce the expectation operator of a quartic term to an effective quadratic term by decoupling the terms along various channels pertinent to the problem. In this particular problem, having an effective spinon-hopping term $\chi_{ij} = \langle f^\dagger_{ij\sigma} f_{ij\sigma} \rangle$ and an effective spinon-pairing term $\Delta_{ij} = \langle f_{i\uparrow} f_{j\downarrow} - f_{i\downarrow} f_{j\uparrow} \rangle$ are relevant. So, we perform a H.S. transformation along these two channels to obtain an effective quadratic Hamiltonian that is easily solvable. This is equivalent in spirit to performing a mean-field decoupling of a system with two-particle interactions to reduce it to a one-particle system responding to an

effective potential that mimics the ensemble averaged behaviour of the entire system.

$$\begin{aligned}
-\frac{1}{4}\left\langle f^\dagger_{i\alpha}f_{j\alpha}f^\dagger_{j\beta}f_{i\beta}\right\rangle =& -\frac{1}{4}\left[\left\langle f^\dagger_{i\alpha}f_{j\alpha}\right\rangle\left\langle f^\dagger_{j\beta}f_{i\beta}\right\rangle+\left\langle f^\dagger_{i\alpha}f_{j\alpha}\right\rangle\left(f^\dagger_{j\beta}f_{i\beta}-\left\langle f^\dagger_{j\beta}f_{i\beta}\right\rangle\right)\right]\\
&-\frac{1}{4}\left\langle f^\dagger_{i\alpha}f_{j\alpha}\right\rangle\left(f^\dagger_{j\beta}f_{i\beta}-\left\langle f^\dagger_{j\beta}f_{i\beta}\right\rangle\right)\\
\approx&\frac{1}{4}(\left\langle f^\dagger_{i\alpha}f_{j\alpha}\right\rangle\left\langle f^\dagger_{j\beta}f_{i\beta}\right\rangle-\left\langle f^\dagger_{i\alpha}f_{j\alpha}\right\rangle f^\dagger_{j\beta}f_{i\beta}-\left\langle f^\dagger_{j\beta}f_{i\beta}\right\rangle f^\dagger_{i\alpha}f_{j\alpha}),\\
=&\frac{1}{4}|\chi_{ij}|^2-\frac{1}{4}\sum_{i,j,\sigma}(\bar{\chi}_{ij}f^\dagger_{i\sigma}f_{j\sigma}+h.c.).
\end{aligned}\tag{4.7}$$

$$\begin{aligned}
-\frac{1}{4}\left\langle\left(f^\dagger_{i\uparrow}f^\dagger_{j\downarrow}-f^\dagger_{i\downarrow}f^\dagger_{j\uparrow}\right)\left(f_{j\downarrow}f_{i\uparrow}-f_{j\uparrow}f_{j\downarrow}\right)\right\rangle =& -\frac{1}{4}(f^\dagger_{i\uparrow}f^\dagger_{j\downarrow}f_{j\downarrow}f_{i\uparrow}+f_{i\downarrow}f_{j\uparrow}f^\dagger_{j\uparrow}f^\dagger_{i\downarrow}-f^\dagger_{i\uparrow}f^\dagger_{j\downarrow}f_{j\uparrow}f_{i\downarrow}\\
&-f_{i\downarrow}f_{j\uparrow}f^\dagger_{j\downarrow}f^\dagger),\\
\approx&-\frac{1}{4}(\langle f^\dagger_{i\uparrow}f^\dagger_{j\downarrow}\rangle f_{j\downarrow}f_{i\uparrow}+\langle f_{j\downarrow}f_{i\uparrow}\rangle f^\dagger_{i\uparrow}f^\dagger_{j\downarrow}+\langle f^\dagger_{i\downarrow}f^\dagger_{j\uparrow}\rangle f_{j\uparrow}f_{i\downarrow}\\
&+\langle f_{j\uparrow}f_{i\downarrow}\rangle f^\dagger_{i\downarrow}f^\dagger_{j\uparrow}-\langle f^\dagger_{i\uparrow}f^\dagger_{j\downarrow}\rangle f_{j\uparrow}f_{i\downarrow}-\langle f_{j\uparrow}f_{i\downarrow}\rangle f^\dagger_{i\uparrow}f^\dagger_{j\downarrow}\\
&-\langle f^\dagger_{i\downarrow}f^\dagger_{j\uparrow}\rangle f_{j\downarrow}f_{i\uparrow}-f^\dagger_{i\downarrow}f^\dagger_{j\uparrow}\langle f_{j\downarrow}f_{i\uparrow}\rangle+\langle f^\dagger_{i\uparrow}f^\dagger_{j\downarrow}\rangle\langle f_{j\downarrow}f_{i\uparrow}\rangle\\
&+\langle f^\dagger_{i\downarrow}f^\dagger_{j\uparrow}\rangle\langle f_{j\uparrow}f_{i\downarrow}\rangle-\langle f^\dagger_{i\uparrow}f^\dagger_{j\downarrow}\rangle\langle f_{j\uparrow}f_{i\downarrow}\rangle-\langle f^\dagger_{i\downarrow}f^\dagger_{j\uparrow}\rangle\langle f_{j\downarrow}f_{i\uparrow}\rangle),\\
=&\frac{J}{4}(\sum_{\langle ij\rangle}\Delta_{ij}(f^\dagger_{i\uparrow}f^\dagger_{j\downarrow}-f^\dagger_{i\downarrow}f^\dagger_{j\uparrow})+h.c.+|\Delta_{ij}|^2).
\end{aligned}\tag{4.8}$$

The action can then be obtained from the Hamiltonian [25]:

$$\begin{aligned}
\mathcal{L}=&\sum_{i,\sigma}\bar{f}_{i\sigma}(\partial_\tau-i\lambda_i)f_{i\sigma}+\sum_i\bar{b}_i(\partial_\tau-i\lambda_i-\mu_B)b_i-\bar{J}\sum_{\langle i,j\rangle}(\bar{\chi}_{ij}\bar{f}_{i\sigma}f_{j\sigma}+h.c.-|\chi_{ij}|^2)\\
&+\bar{J}\sum_{\langle i,j\rangle}(\bar{\Delta}_{ij}(f_{i\uparrow}f_{j\downarrow}-f_{i\downarrow}f_{j\uparrow})+h.c.+|\Delta_{ij}|^2)-\sum_{i,j}t_{ij}\bar{f}_{i\sigma}b_i\bar{b}_jf_{j\sigma}.
\end{aligned}\tag{4.9}$$

The introduction of spinon-hole bound-state particles is achieved by decoupling the last term in the above action using the fermionic H.S. bond fields $F_{ij\sigma}, \bar{F}_{ij\sigma}$. This is equivalent to making the assumption that the low energy excitations of the Fermi surface of the doped Mott insulator are dimers. These quantities carry both spin and charge and they live on the bonds between neighboring lattice sites. They are defined as:

$$\bar{F}_{ij\sigma} := (\bar{f}_{i\sigma}\bar{b}_j + \bar{f}_{j\sigma}\bar{b}_i)/\sqrt{2}. \tag{4.10}$$

This gives us the following action with the dimer terms [24]:

$$\begin{aligned}\mathcal{L} = &\sum_{i,\sigma}\bar{f}_{i\sigma}(\partial_\tau - i\lambda_i)f_{i\sigma} + \sum_i \bar{b}_i(\partial_\tau - i\lambda_i - \mu_B)b_i - \bar{J}\sum_{\langle i,j\rangle}(\bar{\chi}_{ij}\bar{f}_{i\sigma}f_{j\sigma} + h.c. - |\chi_{ij}|^2)\\ &+ \bar{J}\sum_{\langle i,j\rangle}(\bar{\Delta}_{ij}(f_{i\uparrow}f_{j\downarrow} - f_{i\downarrow}f_{j\uparrow}) + h.c. + |\Delta_{ij}|^2) + \sum_{i,j}\bar{F}_{ij\sigma}F_{ij\sigma}\\ &+ \sum_{i,j}\frac{t_{ij}}{\sqrt{2}}(\bar{F}_{ij\sigma}(f_{i\sigma}b_j + f_{j\sigma}b_i) + h.c.).\end{aligned} \tag{4.11}$$

Integrating out the fermionic and bosonic degrees of freedom gives us an effective free energy term that can be written in terms of the order parameters χ, Δ and $F_{ij\sigma}$, along with their Hermitian conjugates. Alternatively, one can use the symmetries in the problem to construct a phenomenological description of the free energy [24]. We get:

$$\begin{aligned}\mathcal{L}_{eff}[\chi_{ij}, \Delta_{ij}, F_{ij\sigma}] = &\sum_{ij}\bar{\chi}_{ij}(\partial_\tau - i(-\lambda_i + \lambda_j)\chi_{ij} + a_1^\chi|\chi_{ij}|^2 + a_2^\chi|\chi_{ij}|^4) + a_3^\chi\sum_{ijkl}\chi_{ij}\chi_{jk}\chi_{kl}\chi_{li}\\ &+ \sum_{ij}\bar{\Delta}_{ij}(\partial_\tau - i(-\lambda_i + \lambda_j)\Delta_{ij} + a_1^\Delta|\Delta_{ij}|^2 + a_2^\Delta|\Delta_{ij}|^4) + a_3^\Delta\sum_{ijkl}\bar{\Delta}_{ij}\Delta_{jk}\bar{\Delta}_{kl}\Delta_{li}\\ &+ \sum_{ij}\bar{F}_{ij\sigma}(\partial_\tau - i(-\lambda_i + \lambda_j))F_{ij\sigma} + a_1^F\bar{F}_{ij\sigma}F_{ij\sigma}\\ &+ \sum_{ijkl}(a_1^{F\chi}\bar{F}_{ij\sigma}F_{jk\sigma}\chi_{kl}\chi_{li} + a_2^{F\chi}\bar{F}_{ij\sigma}\bar{\chi}_{jk}F_{kl\sigma}\chi_{kli} + a_1^{\Delta\chi}\bar{\Delta}_{ij}\Delta_{jk}\chi_{kl}\chi_{li}\\ &+ a_2^{\Delta\chi}\bar{\Delta}_{ij}\bar{\chi}_{jk}\Delta_{kl}\chi_{li}) + \sum_{i,j,k,l}a_1^{F\Delta}\bar{F}_{ij\sigma}F_{jk\sigma}\bar{\Delta}_{kl}\Delta_{li} + a_2^{F\Delta}\bar{F}_{ij\sigma}\Delta_{ij}\bar{\Delta}_{kl}F_{kl\sigma} + ...\end{aligned} \tag{4.12}$$

Here, terms of particular importance for our purposes are the dimer-hopping terms. These terms have coefficients $a_1^{F\Delta}, a_2^{F\Delta}, a_1^{F\chi}, a_2^{F\chi}$... and so on. While imposing the saddle point approximation for the $\mathbb{Z}_2$ fractional Fermi liquid, it is seen that the free energy admits different translationally invariant groundstates. However, we only consider those with s-wave symmetry. It follows that $\langle\chi_{j,\eta}\rangle = \chi$ and $\langle\Delta_{j,\eta}\rangle = \Delta$. As we are working in a phase where spinon-pair condensation is present, we set $\Delta \neq 0$. We are interested in constructing an effective mean-field Hamiltonian where higher order fluctuations of χ and Δ are neglected. The Hamiltonian can then be read out from the effective free-energy and appears to take a form that is reminiscent of the simple tight-binding Hamiltonian. As in [8], we restrict ourselves to three hopping

terms. The Hamiltonian is given by:

$$\begin{aligned}\mathcal{H}_{\mathbb{Z}_2 FL^*} = &- t_1 \sum_{j,\sigma} \bar{F}_{j+\hat{y},x,\sigma} F_{j,x,\sigma} - t_2 \sum_{j\sigma} \bar{F}_{j,y,\sigma} F_{j,x,\sigma} + \\ &- t_3 \sum_{j,\sigma} \bar{F}_{j+\hat{y},y,\sigma} F_{j,x,\sigma} + ...\end{aligned} \tag{4.13}$$

where the dots denote hermitian conjugates, symmetry related, as well as possible longer range hopping terms. The corresponding hopping amplitudes are given by $t_1 = -a_2^{F\Delta}|\Delta|^2 - a_2^{F\chi}|\chi|^2$ and $t_2 = -a_1^{F\Delta}|\Delta|^2 - a_1^{F\chi}|\chi|^2$ and t_3, where t_3 follows from a higher order loop term involving two elementary plaquettes.

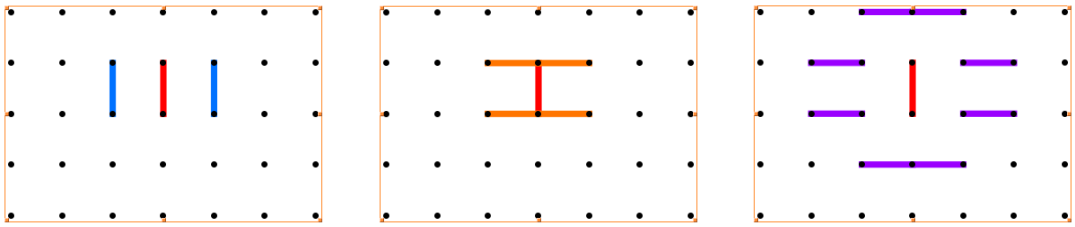

(A) t_1 hopping (B) t_2 hopping (C) t_3 hopping

FIGURE 4.1: Figure illustrates all the different possible hopping configurations that can be achieved by a dimer term that begins in the red configuration and obeys the tight binding Hamiltonian for a $\mathbb{Z}_2$-FL^* system. The hopping configurations shown in blue, orange and purple represent the possible configurations that have hopping amplitudes t_1, t_2 and t_3 respectively.

We now wish to extract the electronic features of the system from the tight-binding Hamiltonian for the $\mathbb{Z}_2$ fractional Fermi liquid. To start off, we diagonalize this Hamiltonian in momentum space and calculate the electronic spectral function of the system.

The tight-binding Hamiltonian of the dimers is written in momentum space in the following manner:

$$\begin{aligned}\mathcal{H} = &- \sum_{k,\sigma} \big(2t_1 \cos(k_x) \bar{F}_{k,x,\sigma} F_{k,x,\sigma} - 2t_1 \cos(k_y) \bar{F}_{k,y,\sigma} F_{k,y,\sigma} - t_2(1 + e^{-ix} + e^{iy} + e^{-i(x+y)}) \bar{F}_{k,x,\sigma} F_{k,x,\sigma} \\ &- t_3(e^{ix} + e^{-i2x} + e^{i(2x-y)} + e^{-iy} + e^{2iy} + 2\cos(x+y) + e^{i(-x+2y)}) \bar{F}_{k,x\sigma} F_{k,y\sigma} + h.c.\big).\end{aligned} \tag{4.14}$$

Diagonalizing the Hamiltonian gives the following two dispersion bands [24]:

$$E_{\pm} = -t_1 s_k \pm \sqrt{t_1^2 d_k^2 + 16 f_k^2 (t_2 + t_3(s_k - 1))^2}, \tag{4.15}$$

where $s_k = \cos k_x + \cos k_y$, $d_k = \cos k_x - \cos k_y$ and $f_k = \cos k_x/2 \cos k_y/2$. The corresponding eigenstates are:

$$\begin{pmatrix} F_{k,x,\sigma} \\ F_{k,y,\sigma} \end{pmatrix} = \begin{pmatrix} v_{+x}(k) & v_{-x}(k) \\ v_{+y}(k) & v_{-y}(k) \end{pmatrix} \begin{pmatrix} F_{k,+,\sigma} \\ F_{k,-,\sigma} \end{pmatrix}, \tag{4.16}$$

where the columns of the matrix form the normalized eigenvectors of the Hamiltonian and can be used to rotate the system from eigenspace to coordinate space. This comes in handy when we want to perform real measurements of the system. Ultimately, we are interested in the electronic properties of the system and would like to have a transformation that takes us from the dimer representation to the electronic representation. This relation is seen in the saddle approximation for χ_{ij} of the gauge invariant electronic field $c_{i\sigma}$, where it can be uniquely expressed in terms of the bond fields Δ_{ij} and $F_{ij\sigma}$ as:

$$c_{i\sigma} \sim \sum_j \bar{F}_{ij\sigma} \Delta_{ij}. \tag{4.17}$$

In momentum space, when $\Delta \neq 0$, this looks like:

$$c_{k\sigma} \sim \Delta \sum_{\eta=x,y} \bar{F}_{-k,\eta,\sigma}(1 + e^{ik_\eta}). \tag{4.18}$$

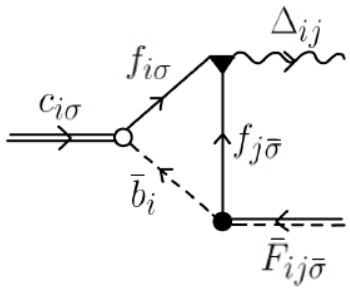

FIGURE 4.2: Electron field $c_{i\sigma}$ in terms of Δ_{ij} and $\bar{F}_{ij\bar{\sigma}}$. Figure from [24].

We can now obtain an expression for the electronic spectral function. The general form of the electronic spectral function [30] is given by :

$$\begin{aligned} A(\vec{k},\omega) &= \frac{2\pi}{\mathcal{Z}}\sum_{n,m}(e^{-\beta E_n} - \zeta e^{-\beta E_m})|\langle n|\hat{c}_k|m\rangle|^2\delta(\omega + E_n - E_m), \\ &= \frac{2\pi}{\mathcal{Z}}\sum_{n,m} e^{-\beta E_n}(1+e^{\beta\omega})|\langle n|\hat{c}_k|m\rangle|^2, \end{aligned} \tag{4.19}$$

where $\mathcal{Z}$ is the partition function of the system. First, we compute $|\langle n|\hat{c}_{k\sigma}|m\rangle|^2$. This is done by replacing the electronic operators with their corresponding representation in dimer space given in equation 4.17. This is then followed by rotating from coordinate space to the eigenspace which diagonalizes the tight binding Hamiltonian of the system. The rotaion matrix is obtained from our calculation in equation 4.16 and leads us to the following result:

$$\begin{aligned} |\langle n|\hat{c}_{k\sigma}|m\rangle|^2 &= \Delta^2\sum_{\eta,\eta'}\langle n|(\bar{v}_{+\eta}\bar{F}_{-k+\sigma} + \bar{v}_{-\eta}\bar{F}_{-k-\sigma})|m\rangle\langle m|(v_{+\eta'}F_{-k+\sigma} + v_{-\eta'}F_{-k-\sigma})|n\rangle \\ &\quad * (1+e^{ik_\eta})(1+e^{-ik_{\eta'}}), \\ &= \Delta^2\sum_{\eta,\eta'}(\bar{v}_{+\eta}v_{+\eta'}\langle n|\bar{F}_{-k+\sigma}|m\rangle\langle m|F_{-k+\sigma}|n\rangle + \bar{v}_{-\eta}v_{-\eta'}\langle n|\bar{F}_{-k-\sigma}|m\rangle\langle m|F_{-k-\sigma}|n\rangle) \\ &\quad * (1+e^{ik_\eta})(1+e^{-ik_{\eta'}}). \end{aligned} \tag{4.20}$$

Using the definition of a weighted average at finite temperatures, we see that:

$$\frac{2\pi}{\mathcal{Z}}\sum_n e^{-\beta E_n}\langle n|\bar{F}_{-k\pm\sigma}F_{-k\pm\sigma}|n\rangle = n_F(\beta E_\pm(-k))\delta(\omega - E_\pm(-k)). \tag{4.21}$$

Plugging this into our expression for the electronic spectral function, we get:

$$A(\vec{k},\omega) = \sum_{\eta,\eta'}(\bar{v}_{+\eta}v_{+\eta'}\delta(\omega - E_+(-k)) + \bar{v}_{-\eta}v_{-\eta'}\delta(\omega - E_-(-k)))(1+e^{ik_\eta})(1+e^{-ik_{\eta'}}) \tag{4.22}$$

The electron spectral function gives the probability density of having an electron with momentum $\vec{k}$ and energy ω. This quantity may be used to explain why Fermi arcs occur. Let us take a system with dimer hopping amplitudes given by $t_1 = -1$, $t_2 = 2$ and $t_3 = -0.6$ as estimated in [8]. We now look at the spectral function near and far away from the nodal point $\vec{k} = (\pi/2, \pi/2)$. Figure 4.3 shows the spectral function that follows after computing equation 4.22.

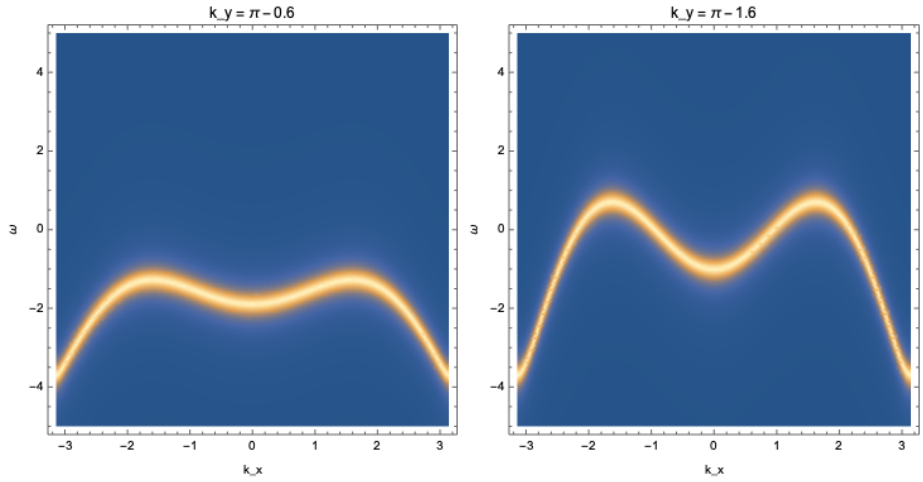

FIGURE 4.3: Plot of the electron spectral function in the $\mathbb{Z}_2$ fractional Fermi liquid phase as a function of momentum k_x for $k_y = \pi - 0.6$ and $k_y = \pi - 1.6$. The δ function in the calculation of the spectral function is replaced by a Lorentzian which broadens the peak for illustration.

Here, we see that when the electron is close to the nodal point $\vec{k} = (\pi/2, \pi/2)$, the electronic spectral function predicts that the energy closes above the Fermi energy thus making room for a closed Fermi surface around the nodal points. But moving away from the nodal points results in the spectral function closing from below the Fermi energy thereby leaving no acceptable energy level at the Fermi momentum. This leaves a gap at the Fermi surface which appears as the pseudogap. Having found the electronic spectral function, we can evaluate the electronic momentum distribution through the following relation:

$$n_k = \int \frac{d\omega}{2\pi} n_F(\omega) A(\vec{k}, \omega). \tag{4.23}$$

4.3 Evaluating correlation functions

In the interest of obtaining correlation functions, what remains for us to do is to choose the dimer resonant amplitudes in equation 4.13 such that they match the conditions set up in the experiment. This can be imposed by considering an effective electronic tight-binding Hamiltonian:

$$\mathcal{H}_0 = -t \sum_{\langle ij \rangle} (c^\dagger_{i\alpha} c_{j\alpha} + h.c). - t' \sum_{\langle\langle ij \rangle\rangle} (c^\dagger_{i\alpha} c_{j\alpha} + h.c.) - t'' \sum_{\langle\langle\langle ij \rangle\rangle\rangle} (c^\dagger_{i\alpha} c_{j\alpha} + h.c.). \tag{4.24}$$

In [7], it is seen that the system has been set up at $U/t = 7.48$ where U is the repulsion between electrons on the same lattice and t is the nearest neighbour hopping

amplitude of electrons (this uses the standard notation used to describe the Hubbard model [30]). We, however, drop the second-nearest-neighbour and third-nearest-neighbour electron hopping term by setting t' and t'' to 0. This is done because the experimental setup is that of an optical lattice with cold atoms where only nearest neighbour hopping i present. The nearest neighbour tight-binding term t is set to 1. This assumption reduces the Hamiltonian to:

$$\mathcal{H}_0 = -\sum_{\langle ij \rangle} (c^\dagger_{i\alpha} c_{j\alpha} + h.c). \tag{4.25}$$

While this is a simple expression for electron-hopping, we are interested in working in dimer space, and so, we require a dimer resonance amplitude term for a dimer tight-binding Hamiltonian of the form in equation 4.13. Following the reasoning presented in [8], it is possible to represent the dimer resonance terms in the following manner:

$$\begin{aligned} t_1 &= -\left\langle 0|F_{iy\uparrow} D_{i+\hat{x},y}|\mathcal{H}_0|D^\dagger_{iy} F^\dagger_{i+\hat{x},y\uparrow}|0\right\rangle, \\ t_2 &= -\left\langle 0|F_{i+\hat{x},y\uparrow} D_{i,y}|\mathcal{H}_0|D^\dagger_{i+\hat{y},x} F^\dagger_{i,x\uparrow}|0\right\rangle, \\ t_3 &= -\left\langle 0|F_{iy\uparrow} D_{i+\hat{x}+\hat{y},x}|\mathcal{H}_0|D^\dagger_{iy} F^\dagger_{i+\hat{x}+\hat{y},x\uparrow}|0\right\rangle, \end{aligned} \tag{4.26}$$

where $D^\dagger_{i,\eta}$ is the creation operator for the spin-singlet term whereas $F^\dagger_{i,\eta\uparrow}$ is the dimer term with a net up-spin magnetization. These terms are defined in terms of electron creation-annihilation operators as given below and can be used to evaluate the matrix elements for the dimer resonance terms. Note that $F^\dagger_{i,\eta\uparrow}$ has already been defined before in equation 4.10 in terms of spinons and holons but we recast the equation in terms of electrons here.

$$D^\dagger_{i,\eta} = \frac{1}{\sqrt{2}}(c^\dagger_{i,\uparrow} c^\dagger_{i+\eta,\downarrow} + c^\dagger_{i+\eta,\uparrow} c^\dagger_{i,\downarrow}|0\rangle, \quad F^\dagger_{i,\eta\alpha} = \frac{1}{\sqrt{2}}(c^\dagger_{i,\alpha} + c^\dagger_{i+\eta,\alpha})|0\rangle. \tag{4.27}$$

Evaluating the matrix elements in equation 4.26 gives the dimer resonance amplitudes $t_1 = -0.5$, $t_2 = 0.5$ and $t_3 = -0.25$. These amplitudes will be utilized for calculating correlations for fractional-Fermi-liquid systems. Using these parameters, the electronic momentum distribution plotted for the fractional Fermi liquid for $\beta = 2$ as a function of the chemical potential μ is shown in Figure 4.4.

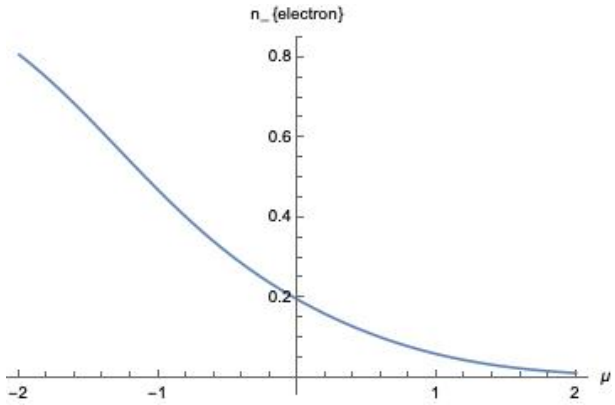

FIGURE 4.4: Electronic momentum distribution for $\mathbb{Z}_2$-FL^* as a function of μ with hopping parameter values $t_1 = -0.5$, $t_2 = 0.5$ and $t_3 = -0.25$ and $\beta = 2$

Now that we have the electronic momentum distribution, we wish to be able to write our correlation function in terms of the electron momentum distribution, so that we may utilize some of the machinery developed earlier. We are interested in evaluating $\left\langle S_i^z S_j^z h_k \right\rangle$.

We know that $S_i^z = \frac{1}{2}(n_{i\uparrow} - n_{i\downarrow})$ is the net magnetization in the system. The hole operator can be evaluated from the constraint that $h_k = 1 - n_{k\uparrow} - n_{k\downarrow}$. Here, we make the simplifying assumption that the contribution to these correlators from doublons is negligible. This assumption was also made earlier in equation 4.3 when the slave-boson formalism was adapted for our particular setup. We need to evaluate the following correlator:

$$\begin{aligned}\left\langle S_i^z S_j^z h_k \right\rangle &= \frac{1}{4}\Big\langle (n_{i\uparrow} - n_{i\downarrow})(n_{j\uparrow} - n_{j\downarrow})(1 - n_{k\uparrow} - n_{k\downarrow}) \Big\rangle, \\ &= \frac{1}{4}\Big\langle n_{i\uparrow}n_{j\uparrow} - n_{i\uparrow}n_{j\downarrow} - n_{i\downarrow}n_{j\uparrow} + n_{i\uparrow}n_{j\downarrow} - n_{i\uparrow}n_{j\uparrow}n_{k\uparrow} \\ &+ n_{i\uparrow}n_{j\downarrow}n_{k\uparrow} + n_{i\downarrow}n_{j\uparrow}n_{k\uparrow} - n_{i\downarrow}n_{j\downarrow}n_{k\uparrow} - n_{i\uparrow}n_{j\uparrow}n_{k\downarrow} + n_{i\uparrow}n_{j\downarrow}n_{k\downarrow} \\ &+ n_{i\downarrow}n_{j\uparrow}n_{k\downarrow} - n_{i\downarrow}n_{j\downarrow}n_{k\downarrow} \Big\rangle.\end{aligned} \tag{4.28}$$

We evaluate each term separately. We shall do this more efficiently by evaluating the general form of the quadratic and cubic density terms, and plugging in the parameters to obtain an expression for each of the above terms. We first look at the general form of the two-body terms alone. While it is not possible to evaluate such an expectation value exactly, we perform a H.S. transformation to get a mean-field description of the required terms. This leads to the following result:

$$\begin{aligned}\left\langle n_{i\sigma_1} n_{j\sigma_2} \right\rangle &= \sum_{\substack{k_1,k_2\\ q_1,q_2}} \frac{1}{V^2} \left\langle c^\dagger_{k_1\sigma_1} c_{k_2\sigma_1} c^\dagger_{q_1\sigma_1} c_{q_2\sigma_1} \right\rangle e^{i((k_1-k_2)r_i+(q_1-q_2)r_j)} \\ &= \sum_{\substack{k_1,k_2\\ q_1,q_2}} \frac{1}{V^2} \Bigg(\left\langle c^\dagger_{k_1\sigma_1} c_{k_2\sigma_1} \right\rangle \left\langle c^\dagger_{q_1\sigma_1} c_{q_2\sigma_1} \right\rangle \delta(k_1-k_2)\delta(q_1-q_2), \\ &\qquad - \left\langle c^\dagger_{k_1\sigma_1} c_{k_2\sigma_1} \right\rangle \left\langle c^\dagger_{q_1\sigma_1} c_{q_2\sigma_1} \right\rangle \delta(k_1-q_2)\delta(q_1-k_2)\delta_{\sigma_1\sigma_2} \Bigg) \\ &\quad * e^{i((k_1-k_2)r_i+(q_1-q_2)r_j)}, \\ &= \left(\frac{n}{2}\right)^2 - \bar{n}^2(r_{ij})\delta_{\sigma_1\sigma_2},\end{aligned} \tag{4.29}$$

where n is the number density of electrons, and

$$\tilde{n}(r_{ij}) = \sum_k \frac{1}{V} \left\langle c^\dagger_{k\sigma} c_{k\sigma} \right\rangle e^{ik(r_i-r_j)}. \tag{4.30}$$

Similarly, the three-body terms are also evaluated. The general Fourier Transform of such a term is:

$$\left\langle n_{i\sigma_1} n_{j\sigma_2} n_{k\sigma_3} \right\rangle = \sum_{\substack{k_1,q_1,p_1\\ k_2,q_2,p_2}} \frac{1}{V^3} \left\langle c^\dagger_{k_1\sigma_1} c_{k_2\sigma_1} c^\dagger_{q_1\sigma_2} c_{q_2\sigma_2} c^\dagger_{p_1\sigma_3} c_{p_2\sigma_3} \right\rangle e^{i((k_1-k_2)r_i+(q_1-q_2)r_j+(p_1-p_2)r_k)}. \tag{4.31}$$

$$
\begin{aligned}
&\bullet \sum_{\substack{k_1,q_1,p_1\\k_2,q_2,p_2}} \frac{1}{V^3}\left\langle \overbrace{c^\dagger_{k_1\sigma_1}}\, c_{k_2\sigma_1}\, \overbrace{c^\dagger_{q_1\sigma_2}}\, c_{q_2\sigma_2}\, \overbrace{c^\dagger_{p_1\sigma_3}}\, c_{p_2\sigma_3}\right\rangle e^{i((k_1-k_2)r_i+(q_1-q_2)r_j+(p_1-p_2)r_k)} = \left(\frac{n}{2}\right)^3.\\
&\bullet \sum_{\substack{k_1,q_1,p_1\\k_2,q_2,p_2}} \frac{1}{V^3}\left\langle \overbrace{c^\dagger_{k_1\sigma_1}}\, c_{k_2\sigma_1}\, \overbrace{c^\dagger_{q_1\sigma_2}\, c_{q_2\sigma_2}\, c^\dagger_{p_1\sigma_3}}\, c_{p_2\sigma_3}\right\rangle e^{i((k_1-k_2)r_i+(q_1-q_2)r_j+(p_1-p_2)r_k)} = -\left(\frac{n}{2}\right)\bar{n}^2(r_{jk})\delta_{\sigma_2\sigma_3}.\\
&\bullet \sum_{\substack{k_1,q_1,p_1\\k_2,q_2,p_2}} \frac{1}{V^3}\left\langle \overbrace{c^\dagger_{k_1\sigma_1}\, c_{k_2\sigma_1}\, c^\dagger_{q_1\sigma_2}}\, c_{q_2\sigma_2}\, \overbrace{c^\dagger_{p_1\sigma_3}}\, c_{p_2\sigma_3}\right\rangle e^{i((k_1-k_2)r_i+(q_1-q_2)r_j+(p_1-p_2)r_k)} = -\left(\frac{n}{2}\right)\bar{n}^2(r_{ij})\delta_{\sigma_1\sigma_2}.\\
&\bullet \sum_{\substack{k_1,q_1,p_1\\k_2,q_2,p_2}} \frac{1}{V^3}\left\langle \overbrace{c^\dagger_{k_1\sigma_1}\, c_{k_2\sigma_1}\, c^\dagger_{q_1\sigma_2}\, c_{q_2\sigma_2}\, c^\dagger_{p_1\sigma_3}}\, c_{p_2\sigma_3}\right\rangle e^{i((k_1-k_2)r_i+(q_1-q_2)r_j+(p_1-p_2)r_k)} = -\left(\frac{n}{2}\right)\bar{n}^2(r_{ik})\delta_{\sigma_1\sigma_3}.\\
&\bullet \sum_{\substack{k_1,q_1,p_1\\k_2,q_2,p_2}} \frac{1}{V^3}\left\langle \overbrace{c^\dagger_{k_1\sigma_1}\, c_{k_2\sigma_1}\, c^\dagger_{q_1\sigma_2}\, c_{q_2\sigma_2}\, c^\dagger_{p_1\sigma_3}\, c_{p_2\sigma_3}}\right\rangle e^{i((k_1-k_2)r_i+(q_1-q_2)r_j+(p_1-p_2)r_k)}\\
&\quad = \bar{n}(r_{ij})\bar{n}(r_{jk})\bar{n}(r_{ik})\delta_{\sigma_1\sigma_2\sigma_3}.\\
&\bullet \sum_{\substack{k_1,q_1,p_1\\k_2,q_2,p_2}} \frac{1}{V^3}\left\langle \overbrace{c^\dagger_{k_1\sigma_1}\, c_{k_2\sigma_1}\, c^\dagger_{q_1\sigma_2}\, c_{q_2\sigma_2}\, c^\dagger_{p_1\sigma_3}\, c_{p_2\sigma_3}}\right\rangle e^{i((k_1-k_2)r_i+(q_1-q_2)r_j+(p_1-p_2)r_k)}\\
&\quad = \bar{n}(r_{ij})\bar{n}(r_{jk})\bar{n}(r_{ik})\delta_{\sigma_1\sigma_2\sigma_3}.
\end{aligned}
\tag{4.32}
$$

Thus, the general Wick's contracted expression for the 3-body term is:

$$
\begin{aligned}
\left\langle n_{i\sigma_1} n_{j\sigma_2} n_{k\sigma_3}\right\rangle = \left(\frac{n}{2}\right)^3 &- \left(\frac{n}{2}\right)\left(\tilde{n}^2(r_{ij})\delta_{\sigma_1\sigma_2} + \tilde{n}^2(r_{jk})\delta_{\sigma_2\sigma_3} + \tilde{n}^2(r_{ik})\delta_{\sigma_1\sigma_3}\right)\\
&+ 2\tilde{n}(r_{ij})\tilde{n}(r_{jk})\tilde{n}(r_{ik})\delta_{\sigma_1\sigma_2\sigma_3}.
\end{aligned}
\tag{4.33}
$$

The unconnected correlation function is obtained by combining all the terms to get :

$$
\left\langle S^z_i S^z_j h_k\right\rangle = \frac{1}{2}(n-1)\tilde{n}^2(r_{ij}) - \tilde{n}(r_{ij})\tilde{n}(r_{jk})\tilde{n}(r_{ik}). \tag{4.34}
$$

It is helpful to first perform these calculations for the simple case of a Fermi liquid. This not only allows us to check the veracity of the expressions we have obtained, but also helps us distinguish those aspects of our results that exhibit non-Fermi behaviour. However, in the case of Fermi liquids, we cannot make the assumption that the effects of having doublons in the system can be ignored. In a half-filled interacting electron system following the t-J model, we have an RVB ground state which admits no naturally occurring doublons. Thus, close to the half-filled state, the effects of doublon interactions are minimal. However, the ground state of a Fermi liquid has a roughly equal probability of having a spin up, spin down, holon, or a doublon, at

any given lattice site if the system is predisposed with zero net-magnetization. So, the doublon density in the system is around 25%. Thus, the effects of doublons in the system cannot be ignored. This is further highlighted by the fact that negative-hole density solutions occur if we naively use the old expression for the hole density, i.e. $h_k = 1 - n_{k\uparrow} - n_{k\downarrow}$.

To remedy this, we see that the electron number density at lattice site k can be viewed as the probability of having one electron on that lattice site. Thus, the hole density at lattice site k is equal to the probability of not having a spin up or a spin down electron at k. $h_k = (1 - n_{k\uparrow})(1 - n_{k\downarrow}) = 1 - n_{k\uparrow} - n_{k\downarrow} + n_{k\uparrow}n_{k\downarrow}$. This is referred to as the Gutzwiller projector.

$$\left\langle S_i^z S_j^z h_k \right\rangle = \frac{1}{4}\left\langle (n_{i\uparrow} - n_{i\downarrow})(n_{j\uparrow} - n_{j\downarrow})(1 - n_{k\uparrow} - n_{k\downarrow} + n_{k\uparrow}n_{k\downarrow}) \right\rangle. \tag{4.35}$$

In a method analogous to the previous case, albeit more cumbersome, we evaluate the spin-spin-hole correlators. The terms that need to be evaluated are:

$$\begin{aligned}
\left\langle S_i^z S_j^z h_k \right\rangle &= \frac{1}{4}\left\langle (n_{i\uparrow} - n_{i\downarrow})(n_{j\uparrow} - n_{j\downarrow})(1 - n_{k\uparrow} - n_{k\downarrow} + n_{k\uparrow}n_{k\downarrow}) \right\rangle, \\
&= \frac{1}{4}\Big\langle n_{i\uparrow}n_{j\uparrow} - n_{i\uparrow}n_{j\downarrow} - n_{i\downarrow}n_{j\uparrow} + n_{i\uparrow}n_{j\downarrow} - n_{i\uparrow}n_{j\uparrow}n_{k\uparrow} \\
&\quad + n_{i\uparrow}n_{j\downarrow}n_{k\uparrow} + n_{i\downarrow}n_{j\uparrow}n_{k\uparrow} - n_{i\downarrow}n_{j\downarrow}n_{k\uparrow} - n_{i\uparrow}n_{j\uparrow}n_{k\downarrow} + n_{i\uparrow}n_{j\downarrow}n_{k\downarrow} \\
&\quad + n_{i\downarrow}n_{j\uparrow}n_{k\downarrow} - n_{i\downarrow}n_{j\downarrow}n_{k\downarrow} + n_{i\downarrow}n_{j\downarrow}n_{k\uparrow}n_{k\downarrow} - n_{i\downarrow}n_{j\uparrow}n_{k\uparrow}n_{k\downarrow} \\
&\quad - n_{i\uparrow}n_{j\downarrow}n_{k\uparrow}n_{k\downarrow} + n_{i\uparrow}n_{j\uparrow}n_{k\uparrow}n_{k\downarrow} \Big\rangle.
\end{aligned} \tag{4.36}$$

The quadratic and cubic density terms can be evaluated in a manner that is identical in form to the expression calculated before. The only additional term of interest is the the quartic term that is evaluated for a general case and is found to be the following:

$$\begin{aligned}\left\langle n_{i\sigma_1} n_{j\sigma_2} n_{k\uparrow} n_{k\downarrow} \right\rangle &= \sum_{\substack{k_1,q_1,p_1,s_1 \\ k_2,q_2,p_2,s_2}} \frac{1}{V^4} \langle c^\dagger_{k_1\sigma_1} c_{k_2\sigma_1} c^\dagger_{q_1\sigma_2} c_{q_2\sigma_2} c^\dagger_{p_1\sigma_3} c_{p_2\sigma_3} c^\dagger_{s_1\sigma_3} c_{s_2\sigma_3} \rangle \\ &\quad * e^{i((k_1-k_2)r_i+(q_1-q_2)r_j+(p_1-p_2+s_1-s_2)r_k)}, \\ &= n_{\sigma_1}\left(n_{\sigma_2} n_\uparrow n_\downarrow - \delta_{\sigma_2\uparrow} \tilde{n}^2_{jk\uparrow} n_\downarrow - \delta_{\sigma_2\sigma_2} \bar{n}^2_{jk\downarrow} n_\uparrow\right) \\ &\quad + \delta_{\alpha\beta} \bar{n}_{ij\sigma_1}\left(-\bar{n}_{ij\sigma_1} n_\uparrow n_\downarrow - \delta_{\sigma_1\uparrow} \bar{n}_{ik\uparrow} \bar{n}_{jk\downarrow} n_\downarrow + \delta_{\sigma_1\downarrow} \bar{n}_{ik\downarrow} n_{jk\downarrow} n_\uparrow\right) \\ &\quad + \delta_{\alpha\uparrow} \bar{n}_{ik\uparrow}\left(\delta_{\sigma_2\uparrow} \bar{n}_{ij\uparrow} \bar{n}_{jk\uparrow} n_\downarrow - \bar{n}_{ik\uparrow} n_\beta n_\downarrow + \delta_{\sigma_2\downarrow} \bar{n}_{ik\uparrow} n^2_{jk\downarrow}\right) \\ &\quad + \delta_{\alpha\downarrow} \bar{n}_{ik\downarrow}\left(\delta_{\sigma_2\downarrow} \bar{n}_{ij\downarrow} \bar{n}_{jk\downarrow} n_\uparrow - \bar{n}_{ik\downarrow} n_\beta n_\uparrow + \delta_{\sigma_2\uparrow} \bar{n}_{ik\downarrow} n^2_{jk\uparrow}\right).\end{aligned} \tag{4.37}$$

Plugging this into our final expression for the correlator and simplifying gives the following result.

$$\left\langle S^z_i S^z_j h_k \right\rangle = (n-1)\bar{n}_{ij}\bar{n}_{ik}\bar{n}_{jk} - \frac{1}{2}(n-1)^2 \bar{n}^2_{ij} - \frac{1}{2}\bar{n}^2_{ik}\bar{n}^2_{jk}. \tag{4.38}$$

4.4 Comparing with Quantum-microscopy experiments

We are now in a position to plot correlation functions for different lattice points around a given dopant and compare the results with experimental data. In order to do this, we are required to fix the temperature of the system and the doping density to match the conditions in which Bloch's experiments [7] were performed. So, we operate at $\beta = 2$ and a hole density $\delta = 5\%$.

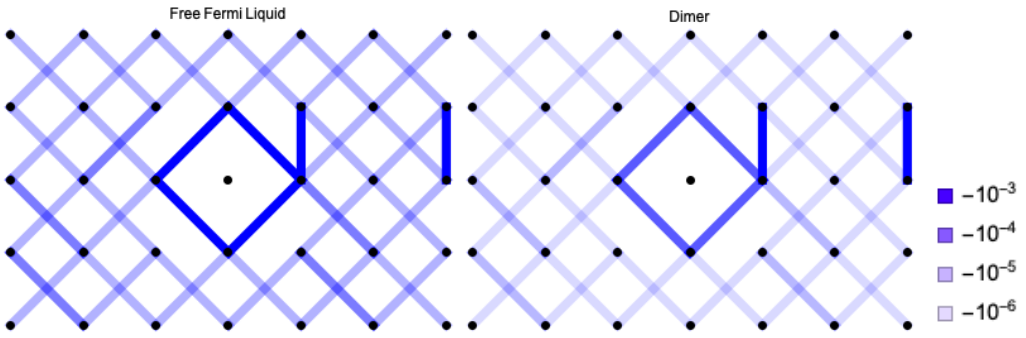

FIGURE 4.5: The figures are the correlation plots around the doped hole in the center of the lattice. The figure on the left is for a free Fermi liquid. The figure on the right is for the Z_2 fractional Fermi liquid. The temperature is set to $\beta = 2$.

There is a clear qualitative difference in the plots that our models give when compared to the plot that is obtained through experiment. The discrepancy seen away from the dopant is particularly striking. While the experiment suggests that there is

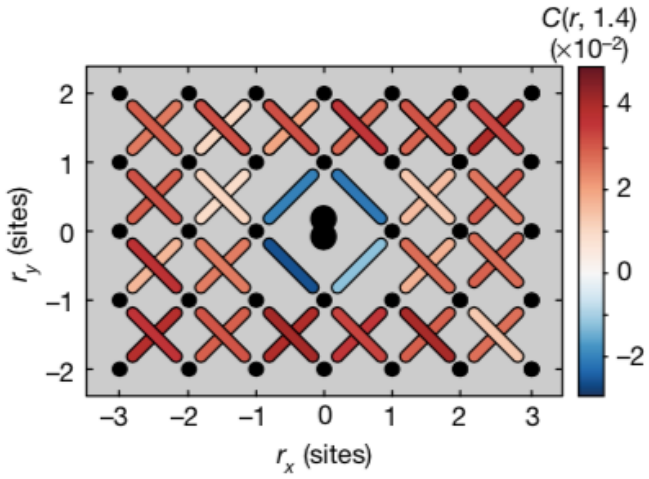

FIGURE 4.6: This figure represents the experimentally observed values obtained by Bloch's group for the spin-spin-hole correlator. Figure from [7].

antiferromagnetic correlation between electrons away from the dopant, this feature is not visible in our models. This is because the fractional-Fermi-liquid model admits an RVB ground-state that does not allow for antiferromagnetic correlations.

We would like to proceed by checking if the polaronic signals grow stronger when one lowers the temperature. $\beta = 2$ is high enough to majorly scramble the Fermi surface of fractional Fermi-liquids. But, extending this evaluation for a smaller temperature may allow us to see if there are greater qualitative similarities to what is seen in Figure 4.6 . Figure 4.7 shows the lattice correlations for $\beta = 20$.

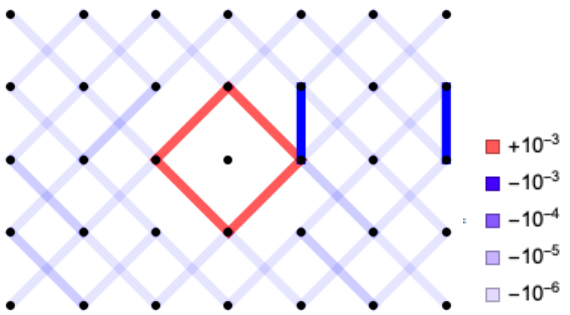

FIGURE 4.7: The figure shows the correlations throughout the lattice predicted by the effective $\mathbb{Z}_2$ fractional Fermi liquid at $\beta = 20$.

The positive correlation for the innermost electrons is unexpected. They appear for temperatures lower than $\beta = 11$ as shown in Figure 4.8. We see a feature that not only shows strong deviations from Fermi behaviour, it is a bold prediction made by the $\mathbb{Z}_2$ fractional Fermi liquid model. Further calculations of these correlators using different models and experimental measurements of this function at temperatures indicated on the graph in Figure 4.8 will certainly lead us to deepening our

understanding of the pseudogap phase.

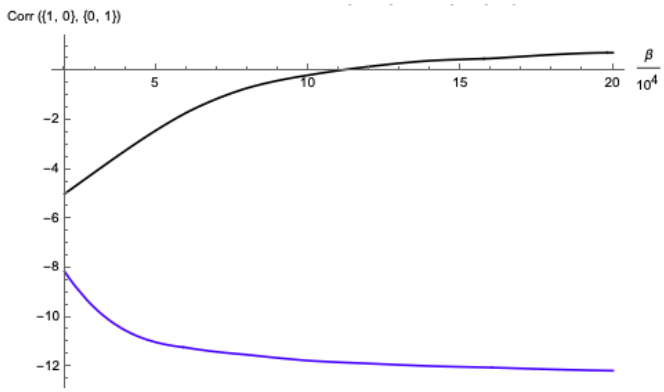

FIGURE 4.8: The correlation between the innermost electrons as a function of inverse temperature for the $\mathbb{Z}_2 FL^*$(black) and the FL(blue) for different inverse temperatures

We hope to gain a little more insight on how differently our model works by comparing it with a few more results obtained by Bloch's group. Bloch's group studied the transition of spin-spin-hole correlators measured on a particular lattice site for different levels of hole-doping [6]. This allows us to test our model with a broad range of hole doping densities.

Before comparing the correlator results to the experiment, we calculate the connected correlator and normalize it in accordance with the paper [6]. The connected correlator is defined in equation 3.4. The normalization is calculated for the cases with and without the Gutzwiller projector. The hole operators are given:

$$\begin{aligned} \langle \hat{h} \rangle &= (1-n) \longrightarrow \text{ w/o Gutzwiller projection,} \\ \langle \hat{h} \rangle &= (1-n+\frac{n^2}{4}) \longrightarrow \text{ with Gutzwiller projection.} \end{aligned} \tag{4.39}$$

The variance of the magnetization can be written as:

$$\begin{aligned} \sigma^2(\hat{S}_2^{\mathbb{Z}}) = \sigma^2(\hat{S}_1^z) = \langle \hat{S}_{r_i}^z \hat{S}_{r_i}^z \rangle &= \frac{1}{4}\langle (n_\uparrow - n_\downarrow)(n_\uparrow - n_\downarrow) \rangle, \\ &= \frac{1}{4}\langle n_\uparrow n_\uparrow + n_\downarrow n_\downarrow - n_\uparrow n_\downarrow - n_\downarrow n_\uparrow \rangle. \end{aligned} \tag{4.40}$$

Let us first evaluate the general expression $\langle n_{\sigma_1} n_{\sigma_2} \rangle$

.

$$\begin{aligned}
\left\langle n_{i\sigma_1} n_{i\sigma_2} \right\rangle &= \sum_{k_1,q_1,k_2,q_2} \frac{1}{V^2} \left\langle c^\dagger_{k_1\sigma_1} c_{k_2\sigma_1} c^\dagger_{q_1\sigma_2} c_{q_2\sigma_2} \right\rangle * e^{i((k_1-k_2)r_i+(q_1-q_2)r_i)} \\
&= \sum_{k_1,q_1,k_2,q_2} \big(\langle c^\dagger_{k_1\sigma_1} c_{k_1\sigma_1} \rangle \langle c^\dagger_{q_1\sigma_2} c_{q_1\sigma_2} \rangle \\
&\qquad + \langle c^\dagger_{k_1\sigma_1} (\delta_{q_1,k_2}\delta_{\sigma_1\sigma_2} - c^\dagger_{q_1\sigma_2} c_{k_2\sigma_1}) c_{q_2\sigma_2} \big) e^{i((k_1-k_2)r_i+(q_1-q_2)r_i)} \\
&= \left(\frac{n}{2}\right)^2 + \sum_{k1} \langle c^\dagger_{k_1\sigma_1} c_{k_1\sigma_2} \rangle \delta_{\sigma_1\sigma_2} - \sum_{k_1,q_1} \langle c^\dagger_{k_1\sigma_1} c_{k_1\sigma_2} \rangle \langle c^\dagger_{q_1\sigma_1} c_{q_1\sigma_2} \rangle, \\
&= \left(\frac{n}{2}\right)^2 + \left(\frac{n}{2} - \left(\frac{n}{2}\right)^2 \right) \delta_{\sigma_1\sigma_2}
\end{aligned} \tag{4.41}$$

From this, the variance is found to be:

$$\sigma^2(\hat{S}^z) = \frac{1}{4}\left(2\left(\frac{n}{2} - \left(\frac{n}{2}\right)^2 \right) \delta_{\sigma_1\sigma_2} \right) = \frac{n}{4} - \frac{n^2}{8}. \tag{4.42}$$

Now, we can plug this into our expression for the normalization constant η and get the following:

$$\begin{aligned}
\eta &= 1/\left(1-n\right)\left(\frac{n}{4} - \frac{n^2}{8}\right) \longrightarrow \text{ w/o Gutzwiller projection,} \\
\eta &= 1/\left(1 - n + \frac{n^2}{4}\right)\left(\frac{n}{4} - \frac{n^2}{8}\right) \longrightarrow \text{ with Gutzwiller projection.}
\end{aligned} \tag{4.43}$$

Thus, our connected correlators for the case with and without Gutzwiller projection is found to be given by:

$$\begin{aligned}
C^c_{3fl^*} &= -\frac{\bar{n}(r_{ij})\bar{n}(r_{jk})\bar{n}(r_{ik})}{(1-n)\left(\frac{n}{4} - \frac{n^2}{8}\right)} \longrightarrow \text{ w/o Gutzwiller projection,} \\
C^c_{3fl} &= \frac{\frac{1}{2}(n-1)\bar{n}(r_{ij})^2 - \bar{n}(r_{ij})\bar{n}(r_{jk})\bar{n}(r_{ik})}{\left(\frac{n}{4} - \frac{n^2}{8}\right)\left(1 - \frac{n}{2}\right)^2} \longrightarrow \text{ with Gutzwiller projection.}
\end{aligned} \tag{4.44}$$

The results in Figure 4.9 provide a platform for many theories to be compared for their relative merits in this particular context, and so, provide an ideal testing ground for the $\mathbb{Z}_2$ fractional Fermi liquid model as well.

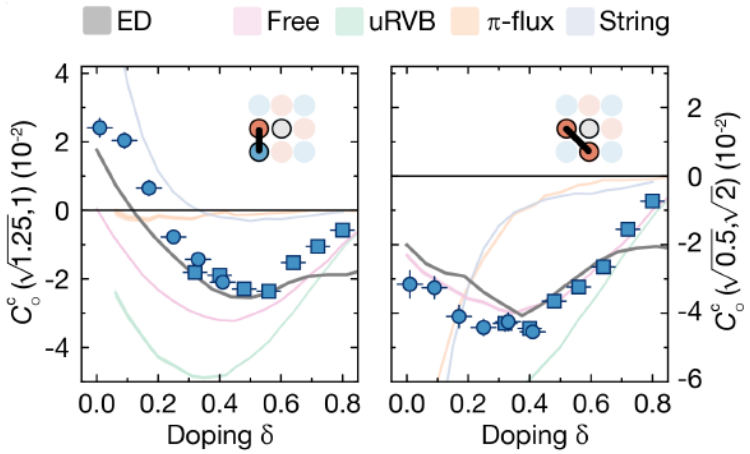

FIGURE 4.9: The correlation functions for the two configurations shown in the image inside the graphs. These are represented by blue points. The diagram also contains different theoretical predictions that one may obtain using the theories mentioned in the color scheme above. In specific, the prediction made by Fermi liquid theory is seen as the pink curve in both plots. Figure from [6]

The curve in the figure was obtained through Monte Carlo simulations [6]. These curves can be compared to the correlators we have constructed for the Fermi-liquid case. We start with a tight-binding Hamiltonian for electrons where the jumping parameter is $t = 1$. The Hamiltonian has the following form:

$$\mathcal{H}_{Fl} = -\sum_{\langle ij \rangle} \hat{c}^{\dagger}_{i\alpha} \hat{c}_{j\alpha} + h.c. \tag{4.45}$$

This gives us the following dispersion relation.

$$\epsilon_k = -2(\cos k_x + \cos k_y). \tag{4.46}$$

With the energy levels at hand, we can obtain the electron-momentum distribution, which is simply the Fermi-Dirac distribution

$$n_k = \frac{1}{1 + e^{\beta(\epsilon_k - \mu)}}. \tag{4.47}$$

Integrating across the entire Brillouin zone reproduces the number-density of the system. The Fourier transformed momentum distribution is obtained by transforming the above expression to real space. Substituting them in our correlators, we can then evaluate equation 4.44 for different hole densities .

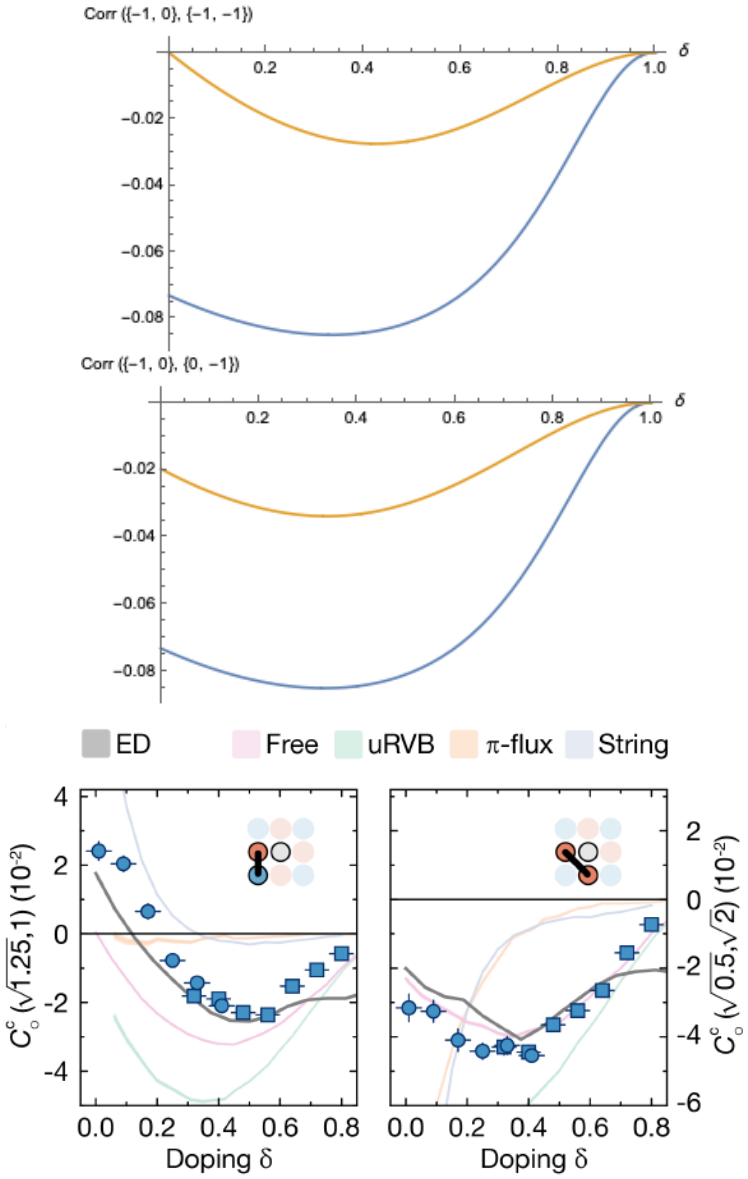

FIGURE 4.10: The top two figures are obtained from the analytical expression of the spin-spin-hole correlator for the Fermi liquid case (yellow) and the $\mathbb{Z}_2 FL^*$ case (blue). The bottom figures are experimental data from reference [6] along with simulations of different models which includes the Monte Carlo simulation of the free Fermi liquid in pink that we are interested in.

Many interesting features are observed in the graphs in Figure 4.10. As far as we can tell by looking at the graphs, the yellow curves (our prediction of the Fermi liquid theory) and the pink curves in Bloch's groups's graphs match reasonably well. This is an encouraging sign as this assures us that the correlators that were constructed are close to what is expected. But we see a huge discrepancy between the $\mathbb{Z}_2$ fractional Fermi liquid correlators and the experimental data. Consider the bottom left graph. For small hole densities, it is seen that the experimental data points show positive correlations for nearest neighbour electrons - A clear break in the antiferromagnetic background of which the system's ground state is a part. The $\mathbb{Z}_2$ fractional Fermi liquid, on the other hand, show strong negative correlations that quite possibly arise out of RVB-ground-state correlations persisting at low doping. This suggests that at this particular regime, the experiment does not admit RVB state correlations that are assumed to exist in the $\mathbb{Z}_2$ frational liquid. The graph on the bottom right shows a qualitatively better match to the blue curves that correspond to the same configuration. However, the Fermi liquid fits the experimental data better here. So we conclude that the correlation signals we expect for a $\mathbb{Z}_2$ fractional Fermi liquid are too strong in comparison to what is actually being seen.

It is not immediately possible to rule out the dimer model as the right model to describe this system. It is conceivable that the Fermi surface is scrambled because of the high temperatures utilized in the experiment. The spinon-hole bound states have a bound-state energy $\sim J$ whereas the Quantum gas microscopy experiments are performed at $\sim 1.4J$. At this temperature, spinon-holon bound-states dissociate to free spinons and holons. In fact, it is even possible that the temperature is too high for the pseudogap phase to manifest. But what kind of features do we observe if the correlations are evaluated at a lower temperature? Even if our results get no closer to what Bloch observes, it is possible that later experiments at lower temperatures could validate the dimer model. And so, we explore the behaviour of these correlators at lower temperatures. We have chosen $\beta = 20$ and $\beta = 200$.

It is seen in Figure 4.11 that in all the four blue curves that a positive correlation. This is interesting because this suggests that the $\mathbb{Z}_2$ fractional Fermi liquid has a strong predisposition to align neighbouring spins along the same direction in the vicinity of a hole at low hole doping densities. The small positive correlation that appears at lower temperatures suggest that the $\mathbb{Z}_2$ fractional Fermi liquid is capable of exhibiting a sign-flip if the temperatures are low enough. While this may not represent the same sign-flip that Bloch's group observes, it may be a verifiable prediction if the experiment was performed at lower temperatures. On the other hand, it may turn out that the regimes are entirely different, and what we are seeing may not be realizable on an optical lattice with cold atoms.

The disparity between the experimental data and our results can be accounted for by the fact that next to nearest neighbour hopping of electrons plays a crucial role in explaining pseudogap phenomena. One reason why this interaction is important for pseudogap phenomena is that the next to nearest neighbour hopping imparts a dispersion to the doped holes and this subtly alters the energetics of the system [31]. However, since the experimental setup is built on an optical lattice with cold atoms,

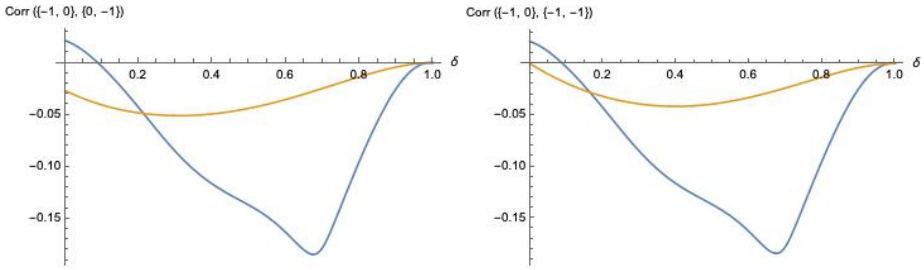

(A) The two figures represent correlations evalueted at $\beta = 20$. The figure on the left measures innermost diagonal correlation of electrons while the figure on the right represents nearest neighbour correlations for the innermost electrons

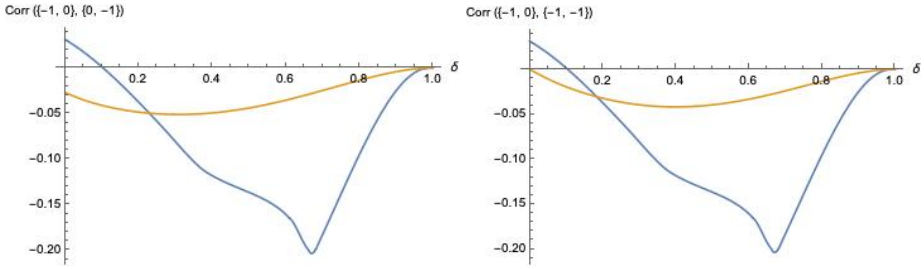

(B) The two figures represent correlations evalueted at $\beta = 200$. The figure on the left measures innermost diagonal correlation of electrons while the figure on the right represents nearest neighbour correlations for the innermost electrons.

FIGURE 4.11: The yellow curve is our prediction of the Fermi liquid while the blue curve gives our prediction for the $\mathbb{Z}_2$ fractional Fermi liquid.

any hopping beyond nearest neighbours is negligible. So, it might very well be that the pseudogap regime is not realizable in this set-up. But these results are useful because they predict that a sign flip in the innermost correlations is observed at temperatures lower than $\beta = 11$. Future experiments performed at lower temperatures that allow for next-to-nearest hopping will be able to directly test this prediction.

Chapter 5

Slave boson mean field theory with spinon/holon excitations

In this chapter, we move on to our next problem of interest. Our goal is to understand the different phases of matter that arise if the low energy excitations of the t-J model were a mixture of free spinons/ holons and spinon-holon bound-state excitations. We hope to study such a system by obtaining its free energy and minimizing it with respect to the order parameters present in the system. This provides us with self-consistent equations which we can solve to obtain the exact dependence of the order parameters as a function of hole-density. Before looking at the general case with multiple low energy excitations, it is instructive to initially study the simple case of having just the free spinon/holon excitations. We dedicate this chapter to study the phases of the t-J model with spin-charge separation (free spinon/ holon excitations).

As a first step, it is instructive to understand the role of the spinon-pair condensate in the Hamiltonian of our mixed system. It is also relevant to acquaint ourselves with the concept of Bogoliubov quasiparticles. So, we look at the derivation of the BCS mean-field theory.

5.1 BCS mean field theory

When an electron moves through a lattice, it distorts the cations on the lattice sites around it creating quantized lattice oscillations known as phonons which pass through the lattice and interact with other electrons. One can demonstrate that an effective long-range attractive interaction can develop between electrons of opposite spins mediated by phonons [20]. This long-range interaction creates a bound-state of two electrons with opposite spins that are referred to as a Cooper pair. In order to study them, we we construct an attractive pseuduopotential between such electrons that models the phonon mediated attraction. Let us assume an interacting Hamiltonian of the form $\mathcal{H}_{int} = -g\hat{\delta}(x)$. Converting to momentum space and writing in second quantized formalism, the Hamiltonian becomes:

$$\mathcal{H} = \sum_{k,\sigma} \bar{c}_{k\sigma}(\epsilon_k - \mu)c_{k\sigma} - \frac{g}{V}\sum_{k,q,Q} \bar{c}_{Q+q,\uparrow}\bar{c}_{-q,\downarrow}c_{-k,\downarrow}c_{Q+k,\uparrow}, \tag{5.1}$$

where $c^{\dagger}_{k\sigma}$ is the electronic creation operator, ϵ_k is the free particle dispersion, μ is the chemical potential and g is the interaction strength. We want to perform a mean-field decoupling of the action that has terms that have been decoupled along the Cooper-pairing channel. In order to do so, let us define a Cooper pair creation operator [30]:

$$\bar{\Delta}_Q := \frac{g}{V}\sum_k \bar{c}_{k+Q,\uparrow}\bar{c}_{-k,\downarrow}. \tag{5.2}$$

Below a critical temperature, Δ_Q condenses such that all the Cooper pairs settle at the zero-momentum state. Performing a mean-field decoupling of the quartic spinon-operator reduces the interacting Hamiltonian to an effective quadratic operator given by:

$$\begin{aligned}
\mathcal{H}_{int} &= -\frac{g}{V}\sum_{k,q,Q}\bar{c}_{Q+q,\uparrow}\bar{c}_{-q,\downarrow}c_{-k,\downarrow}c_{Q+k,\uparrow} \\
&\approx -\frac{V}{g}\sum_Q(\bar{\Delta}_Q\langle\Delta_Q\rangle + \langle\bar{\Delta}_Q\rangle\Delta_Q - \langle\bar{\Delta}_Q\rangle\langle\Delta_Q\rangle) \\
&= -\sum_k(\Delta\bar{c}_{k\uparrow}\bar{c}_{-k\downarrow} + h.c.) + \frac{V}{g}|\Delta|^2, \qquad \big(\text{using the ansatz } \langle\hat{\Delta}_Q\rangle = \Delta\delta_{Q,0}\big).
\end{aligned} \tag{5.3}$$

The entire matrix can then be written in Nambu spinor notation in the following manner:

$$\begin{aligned}
\mathcal{H}(\Delta^*,\Delta) &= \sum_{k,\sigma}\bar{c}_{k\sigma}(\epsilon_k-\mu)c_{k\sigma} - \sum_k(\Delta_k\bar{c}_{k\uparrow}\bar{c}_{-k\downarrow} + h.c.) + \frac{V}{g}|\Delta|^2, \\
&= \sum_k \begin{pmatrix}\bar{c}_{k\uparrow} & c_{-k\downarrow}\end{pmatrix} \overbrace{\begin{pmatrix}\epsilon_k-\mu & \Delta \\ \bar{\Delta} & \mu-\epsilon_{-k}\end{pmatrix}}^{H} \begin{pmatrix}c_{k\uparrow} \\ \bar{c}_{-k\downarrow}\end{pmatrix} + \sum_k(\epsilon_k-\mu) + \frac{V}{g}|\Delta|^2.
\end{aligned} \tag{5.4}$$

We diagonalize the above matrix through a Bogoliubov transformation which 'rotates' the coordinate system to a frame of reference that diagonalizes the Hamiltonian. This constitutes defining a new set of creation-annihilation operators that are written as a linear combination of the electronic operators and obey fermionic-anticommutation relations. The constituent quasiparticles are referred to as the Bogoliubov quasiparticles. They are written as:

$$\begin{pmatrix}\gamma_{k\uparrow} \\ \bar{\gamma}_{-k\downarrow}\end{pmatrix} = \begin{pmatrix}\cos\theta_k & \sin\theta_k \\ -\sin\theta_k & \cos\theta_k\end{pmatrix}\begin{pmatrix}c_{k\uparrow} \\ \bar{c}_{-k\downarrow}\end{pmatrix} = M\begin{pmatrix}c_{k\uparrow} \\ \bar{c}_{-k\downarrow}.\end{pmatrix} \tag{5.5}$$

where θ_k is an angle that is chosen so as to diagonalize the Hamiltonain. Setting

$\Delta \in \mathbb{R}$, the Hamiltonian can be written as:

$$\mathcal{H} = \sum_{k,\sigma} \begin{pmatrix} \bar{\gamma}_{k\uparrow} & \gamma_{-k\downarrow} \end{pmatrix} MHM^{\dagger} \begin{pmatrix} \gamma_{k\uparrow} \\ \bar{\gamma}_{-k\downarrow} \end{pmatrix} + \sum_{k} (\epsilon_k - \mu) + \frac{V}{g} |\Delta|^2. \tag{5.6}$$

We now find an appropriate θ_k that diagonalizes the Hamiltonian. We see that:

$$MHM^{\dagger} = \begin{pmatrix} (\epsilon_k - \mu)\cos 2\theta_k - \Delta \sin 2\theta_k & -(\epsilon_k - \mu)\sin 2\theta_k - \Delta \cos 2\theta_k \\ -(\epsilon_k - \mu)\sin 2\theta_k - \Delta \cos 2\theta_k & -(\epsilon_k - \mu)\cos 2\theta_k + \Delta \sin 2\theta_k \end{pmatrix}. \tag{5.7}$$

This gives $\tan 2\theta_k = -\dfrac{\Delta}{\epsilon_k - \mu}$.

$$\implies \cos 2\theta_k = \frac{\epsilon_k - \mu}{\sqrt{(\epsilon_k - \mu)^2 + \Delta^2}}, \quad \text{and} \quad \sin 2\theta_k = \frac{\Delta}{\sqrt{(\epsilon_k - \mu)^2 + \Delta^2}}, \tag{5.8}$$

The final BCS mean-field Hamiltonian reads:

$$\mathcal{H}_{MF} = \sum_{k,\sigma} E_k \bar{\gamma}_{k\sigma} \gamma_{k\sigma} + \sum_{k} (\epsilon_k - \mu) + \frac{V}{g} |\Delta|^2, \tag{5.9}$$

where $E_k = \sqrt{(\epsilon_k - \mu)^2 + \Delta^2}$ is the quasiparticle dispersion with an energy gap of Δ.

For the purposes of this thesis, we are interested in the zero-temperature momentum distribution of the electrons. This is found to be:

$$\begin{aligned} n_F(k) &= \langle c^{\dagger}_{k\uparrow} c_{k\uparrow} \rangle, \\ &= \langle (\cos\theta_k \gamma^{\dagger}_{k\uparrow} - \sin\theta_k \gamma_{-k\downarrow})(\cos\theta_k \gamma_{k\uparrow} - \sin\theta_k \gamma^{\dagger}_{-k\downarrow}) \rangle, \\ &= \sin^2\theta_k + \cos 2\theta_k \langle \gamma^{\dagger}_{k\uparrow} \gamma_{k\uparrow} \rangle, \end{aligned} \tag{5.10}$$

where $n_F(k)$ is the momentum distribution of the electron. From the trigonometric relations derived in equation 5.8, we set the temperature of the system to zero and obtain:

$$n_F(k) = \frac{1}{2}\left(1 - \frac{\epsilon_k - \mu}{E_k}\right). \tag{5.11}$$

5.2 Free energy derivation

Consider the t-J model with spin-charge separation, that is, a model where the spinons and holons have free particle dispersions. Such a system has sufficient information to capture many properties exhibited by the doped Mott insulator, while at the same time being simple enough to work with. For this calculation, we closely follow the discussion presented in Koliar and Liu (1989) [4]. First, we explore the zero temperature behaviour of the order parameters. This gives a qualitative idea as to where the critical temperatures are located. Consider the spinon-pairing field Δ which couples free spinons of opposite spin. But , due to thermal fluctuations, there is a tendency for singlet pairs to dissociate back into free spinons. There is a tug-of-war between entropy and the phonon-mediated attractive interaction set up in the system. So, the critical temperature for spinon-pairs to dissociate can be expected to have the same order of magnitude as the spinon-pairing strength at zero temperature.

To start off, we perform a mean-field analysis of the t-J model in the slave boson formalism introduced in equation 4.6 . Here, in the interest of comparing our results with Kotliar and Liu [4], we employ the same definitions for the pertinent fields in the problem. The new order parameters we choose are defined as:

$$\begin{aligned}
\chi_x &= \frac{3J}{2}\langle f^\dagger_{i,\sigma} f_{i+x,\sigma}\rangle, \\
\chi_y &= \frac{3J}{2}\langle f^\dagger_{i,\sigma} f_{i+y,\sigma}\rangle, \\
\Delta_x &= \frac{3}{2}\langle f_{i\uparrow} f_{i+\hat{x}\downarrow} - f_{i\downarrow} f_{i+\hat{x}\uparrow}\rangle, \\
\Delta_y &= \frac{3}{2}\langle f_{i\uparrow} f_{i+\hat{y}\downarrow} - f_{i\downarrow} f_{i+\hat{y}\uparrow}\rangle.
\end{aligned} \tag{5.12}$$

It was discussed in the derivation of equation 4.6 that the t-J Hamiltonian in the slave-boson formalism is written as :

$$\begin{aligned}
\mathcal{H} = \sum_{\langle ij\rangle} \Big[J\big[&-\frac{1}{4}\bar{f}_{i\alpha} f_{j\alpha} \bar{f}_{j\beta} f_{i\beta} - \frac{1}{4}(\bar{f}_{i\uparrow}\bar{f}_{j\downarrow} - \bar{f}_{i\downarrow}\bar{f}_{j\uparrow})(f_{j\downarrow} f_{i\uparrow} - f_{j\uparrow} f_{i\downarrow}) + \frac{1}{4}\bar{f}_{i\alpha} f_{j\alpha}\big] \\
&- \frac{1}{4}(1-\bar{b}_i b_i)(1-\bar{b}_j b_j)\Big] - t\sum_{ij\sigma}(\bar{f}_{i\sigma} b_i \bar{b}_j f_{j\sigma} + h.c.).
\end{aligned} \tag{5.13}$$

Performing the H.S. transformation in a manner similar to equations 4.7 and 4.8, we get the following result:

$$-\frac{1}{4}\left\langle \bar{f}_{i\alpha}f_{j\alpha}\bar{f}_{j\beta}f_{i\beta}\right\rangle \approx \frac{1}{9J^2}|\chi_{ij}|^2 - \frac{1}{6J}\sum_{i,j,\sigma}(\bar{\chi}_{ij}\bar{f}_{i\sigma}f_{j\sigma} + h.c.)$$
$$-\frac{1}{4}\left\langle \left(\bar{f}_{i\uparrow}\bar{f}_{j\downarrow} - \bar{f}_{i\downarrow}\bar{f}_{j\uparrow}\right)\left(f_{j\downarrow}f_{i\uparrow} - f_{j\uparrow}f_{j\downarrow}\right)\right\rangle \approx \frac{1}{6J}\Big(\sum_{\langle ij\rangle}\Delta_{ij}(\bar{f}_{i\uparrow}\bar{f}_{j\downarrow} - \bar{f}_{i\downarrow}\bar{f}_{j\uparrow}) + h.c.\Big) + \frac{1}{9J^2}|\Delta_{ij}|^2. \tag{5.14}$$

The spinon-holon-interaction term cannot be transformed using a fermionic H.S. transformation. Here, we make the simplifying assumption that the holons are all condensed in the zero momentum state. A condensate of holons has an extensive number of holons in a single particle state that leads to the result described below.

$$\begin{aligned} b^\dagger|n\rangle &= \sqrt{n+1}|n+1\rangle \approx \sqrt{n}|n\rangle, \\ \implies \langle n|b^\dagger|n\rangle &\approx \sqrt{n}. \end{aligned} \tag{5.15}$$

Here $|n\rangle$ refers to the Fock-state with n bosons in the ground state and none in the higher energy states. The operator $b^\dagger$ represents any bosonic creation operator. The spinon-holon-interaction term then gives:

$$-t\sum_{ij\sigma}(\bar{f}_{i\sigma}b_i\bar{b}_jf_{j\sigma} + h.c.) \approx -t\sum_{ij\sigma}\bar{f}_{i\sigma}f_{j\sigma}\delta \tag{5.16}$$

where δ, which counts the holons in the zero momentum state is given by $\sqrt{\delta} \sim \langle b_i^\dagger\rangle$. Another modification made to the Hamiltonian is that we multiply it by a factor of $6J$. The spinon-holon interaction term t and the Matsubara frequency terms that come when writing the action are transformed such that the entire action scales by a constant factor. This does not affect the subsequent minimization of the free energy as the location of its local extrema are still preserved. This reduces the Hamiltonian to [4]:

$$\begin{aligned} \mathcal{H}_0 = &-\sum_{i\sigma}[\chi_x f_{i,\sigma}^\dagger f_{i+\hat{x},\sigma} + \chi_y f_{i,\sigma}^\dagger f_{i+\hat{y},\sigma} + h.c.] + \sum_i[\Delta_x^\dagger(f_{i\uparrow}f_{i+\hat{x}\downarrow} - f_{i\downarrow}f_{i+\hat{x}\uparrow}) + h.c.] \\ &+\sum_i[\Delta_y^\dagger(f_{i\uparrow}f_{i+\hat{y}\downarrow} - f_{i\downarrow}f_{i+\hat{y}\uparrow}) + h.c.] - \delta t\sum_{\langle ij\rangle\sigma}(f_{i\sigma}^\dagger f_{j,\sigma} + h.c.) + \frac{2}{3J}\sum_{\langle ij\rangle}(|\Delta_{ij}|^2 + |\chi_{ij}|^2). \end{aligned} \tag{5.17}$$

It follows that the partition function before integration takes the form:

$$\mathcal{Z} = \int \mathcal{D}[\bar{f},f]e^{-\int_0^\beta d\tau(\sum_{i=1}^N \bar{f}_i(\tau)\partial_\tau f_i(\tau) + \mathcal{H}_0[\bar{f},f] - \mu\hat{N}[\bar{f},f])}, \tag{5.18}$$

where we have defined $\mathcal{D}[\bar{f},f] = \lim_{M\to\infty}\prod_{n=0}^M d[\bar{f},f]$. Now, we perform the above functional integral and deduce the corresponding free energy of the system from the standard thermodynamic relation $\mathcal{F} = -(1/\beta)\log\mathcal{Z}$. The free energy is

found to be [4]:

$$\mathcal{F} = -2T\sum_k \log\cosh(\beta E_k/2) - \mu N + \frac{2N}{3J}(|\chi_x|^2 + |\chi_y|^2 + |\Delta_x|^2 + |\Delta_y|^2) \tag{5.19}$$

where $\chi_x = |\chi_x|e^{i\alpha_x}$, $\chi_y = |\chi_y|e^{i\alpha_y}$, $\Delta_x = |\Delta_x|e^{\beta_x}$, $\Delta_y = |\Delta_y|e^{i\beta_y}$, and $\theta := \beta_y - \beta_x$.

Here α_i, β_i represent angles that we obtain when we parametrize the orderparameters in polar coordinates.

We also have $E_k = \sqrt{(\epsilon_k - \mu)^2 + 4|\Delta_k|^2)}$, where $\epsilon_k = -\delta t K_k - 2(|\chi_x|\cos(k_x a - \alpha_x) + |\chi_y|\cos(k_y a - \alpha_y)$, $\Delta_k = 2(\Delta_x \cos k_x a + \Delta_y \cos k_y a)$ and $K_k = 2(\chi_x \cos k_x a + \chi_y \cos k_y a)$.

Particle conservation imposes:

$$1 - \delta = \sum_\sigma \langle f^\dagger_{i\sigma} f_{i\sigma}\rangle. \tag{5.20}$$

5.3 Phase diagram for spinon/holon excitations

The different phases of matter exhibited by the system can be inferred by solving the equations that result from minimizing the free energy given in equation 5.19. As a first step, the number of variables in equation 5.19 is reduced by noticing that the following constraints minimize the free energy [4]:

$$\begin{aligned} &\alpha_x = \alpha_y = 0, \\ &\chi_x = \chi_y := \chi, \\ &|\Delta_x| = -|\Delta_y| := \pm|\Delta|, \\ &\theta = \pi. \end{aligned} \tag{5.21}$$

We can now minimize the free energy with respect to the order parameters $\bar{\Delta}$ and $\bar{\chi}$ and obtain the following self-consistent equations at zero temperature.

$$\chi = -\frac{3J}{8N}\int_{-\pi}^{\pi}\frac{d^2k}{4\pi^2}\frac{(\epsilon_k - \mu)}{E_k}K_k, \tag{5.22}$$

$$1 = \frac{3J}{8N}\int_{-\pi}^{\pi}\frac{d^2k}{4\pi^2}\frac{2\Gamma_k^2}{E_k}. \tag{5.23}$$

where $\Gamma_k = \Delta(\cos k_x - \cos k_y)$. A third equation is obtained from evaluating the RHS of equation 5.20 at zero temperature. The exact expression is derived here:

$$\langle \delta \rangle = \int_{-\pi}^{\pi} \frac{d^2k}{4\pi^2}(1 - 2n_F(E_k)), \tag{5.24}$$

where $n_f(E_k)$ is the momentum distribution of the electron as calculated in equation 5.11 (Note that this is not the Fermi-Dirac distribution). Using this, we calculate the hole density distribution to be:

$$\delta = \int_{-\pi}^{\pi} \frac{d^2k}{4\pi^2}\left(\frac{\epsilon_k - \mu}{E_k}\right). \tag{5.25}$$

This forms the third self-consistent equation that needs to be solved. Now that we have three equations and three variables, we can solve the equations to find out how the coupling strength of the spinon pairs changes with hole density.

Setting $N, J = 1$ and $t = 10$ [4], the self-consistent equations are solved by a fixed point iteration scheme. Here, guess values for χ, δ and Δ are plugged into equations 5.22, 5.23 and 5.25 and and their values are iteratively updated until they converge. This calculation is then repeated by changing the chemical potential until we have sufficient data points to plot a $\Delta(\delta)$ curve and $\chi(\delta)$ curve. The following curves in Figure 5.1 are obtained at the end of this procedure.

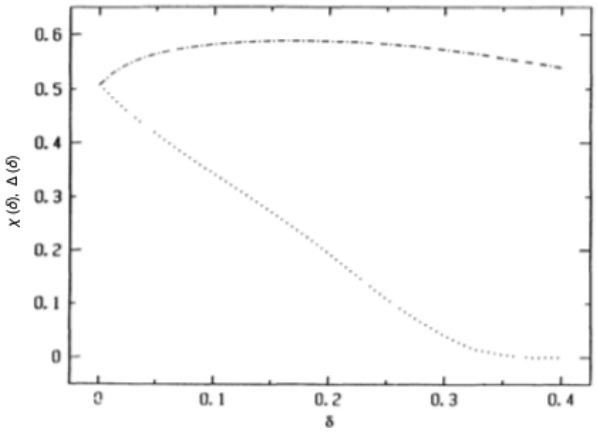

FIGURE 5.1: Figure illustrates two different curves, χ and Δ as a function of hole density δ at zero temperature. The dashed line is $\chi(\delta)$ while the dotted line is $\Delta(\delta)$. Figure from [4]

It is seen from this curve that χ is nearly independent of the hole density as it consistently hovers above 0.5. $\Delta(\delta)$, however, decays with hole doping. It is seen

that spinon-pairing disappears at around 35% hole doping. As argued before, we expect a very similar trend when looking at the critical temperature for the spinon-pair condensate.

We are now in a position to calculate the critical temperature for the spinon-pairs to condense as a function of δ. It is our goal to obtain the phase diagram of the 2D t-J model in the slave-boson representation that are permeated by spinons and holons.

For this problem, however, the unknowns are T_c, δ and χ. Δ is, by definition, zero at the critical temperature. As Δ is zero, there are no off-diagonal elements in the Nambu matrix and we are free to use the Fermi-Dirac distribution for the momentum density of electrons. Our self-consistent equations then read:

$$\chi = -\frac{3J}{8N}\int_{-\pi}^{\pi}\frac{d^2k}{4\pi^2}K_k \tanh\left(\frac{\epsilon_k-\mu}{2T_c}\right), \tag{5.26}$$

$$1 = \frac{3J}{8N}\int_{-\pi}^{\pi}\frac{d^2k}{4\pi^2}\frac{2\Gamma_k^2}{\epsilon_k-\mu}\tanh\left(\frac{\epsilon_k-\mu}{2T_c}\right), \tag{5.27}$$

$$\delta = \frac{1}{N}\int_{-\pi}^{\pi}\frac{d^2k}{4\pi^2}\tanh\left(\frac{\epsilon_k-\mu}{2T_c}\right). \tag{5.28}$$

Solving these equations through fixed-point iteration, one obtains Figure 5.2 :

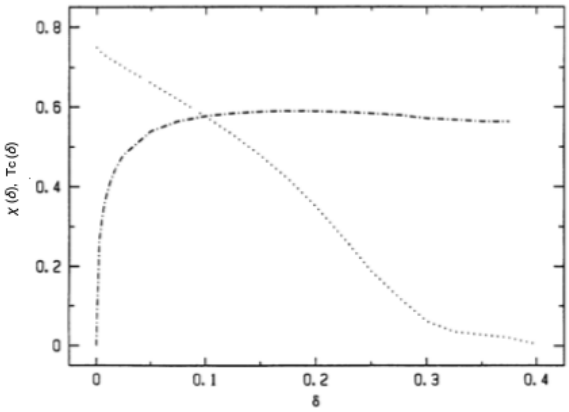

FIGURE 5.2: Figure illustrates two different curves, χ and T_c as a function of hole density δ at the temperature. T_c is the critical tempearture for the spinon-pair condensate to form. The dashed line is $\chi(\delta)$ while the dotted line is $T_c(\delta)$. Figure from [4].

We can see a qualitative similarity between Figure 5.1 and 5.2. While the critical temperature was larger than the anticipated at $\delta = 0$, it decays to zero at around the same hole-density. The graph is steeper, but the initial guess retains all the essential features of the actual curve.

Finally, all that remains is to calculate the holon condensation temperature as a function of a hole doping for which the results obtained in [4] are displayed. It is seen that holon condensation, like any bosonic condensation, does not occur at finite temperatures in 2D systems. But, even the introduction of a tiny interlayer hopping in the holon dispersion relation gives a non-zero holon-condensation temperature. The holonic tight binding dispersion looks like $\epsilon_k = -t_b(2\cos k_x + 2\cos k_y + r_z \cos k_z)$. This temperature is not very sensitive to the choice of r_z as it only scales logarithmically [21,22], and even a choice of $r_z \sim 0.1t_b$ is sufficient to give the desired results.

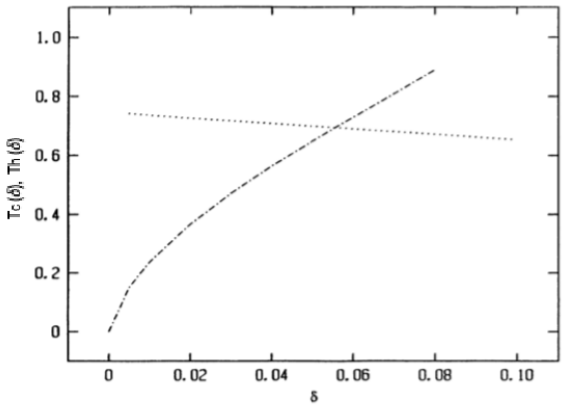

FIGURE 5.3: Figure illustrates two different curves, T_c and T_h as a function of hole density δ. T_c, T_h are the spinon-pairing and holon condensation temperatures respectively. The dashed line is $T_h(\delta)$ while the dotted line is $T_c(\delta)$ Figure from [4].

As the dashed line and dotted lines cross each other, one sees four different phases of matter manifesting in Figure 5.3. A fifth phase is also seen in Figure 5.2 where one observes the $\chi = 0$ phase above the dashed line. So, combining all the features that this system is showing, we have the following diagram that catpures the different phases of matter:

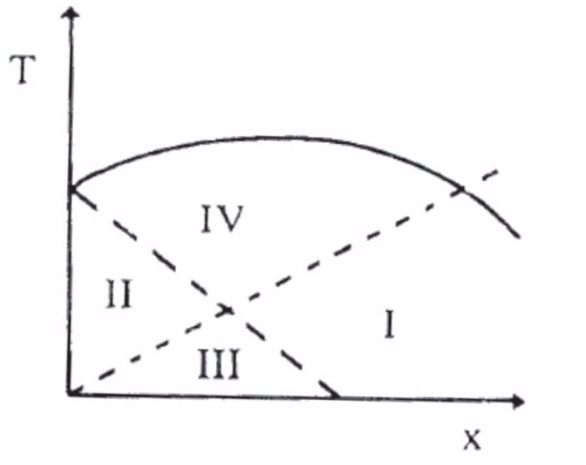

FIGURE 5.4: Figure illustrates the different phases of matter that our system exhibits. The curve on the top demarcates the $\chi = 0$ phase. The dashed line with a positive slope corresponds to the critical temperature for holon condensation whereas the dashed line with the negative slope corresponds to the critical temperature of the spinon-pair-condensates ($\Delta = 0$). Figure from [25].

As seen in Figure 5.4, the incoherent phase $\chi = 0$ is seen at high temperatures when there is no spinon hopping and all order parameters are zero. In the uniform RVB state (IV in Figure 5.4), only χ is nonzero, while $\Delta, \delta = 0$, while in the spin-gap state (II), $\delta = 0$. This corresponds to a state where none of the holes are condensed which gives rise to incoherent charge-dynamics. The superconducting state cannot occur in these conditions as it requires the holons to condense as well. This can be interpreted as the pseudogap phase, a state that is a precursor to the superconductor [23]. (I) is characterized by free spinons and holons none of which condense. This gives rise to classic Fermi-liquid behaviour as there are no off-diagonal terms in the Hamiltonian in this regime. It is in regime (III) that superconductivity is exhibited as there is both spinon pairing and holon condensation. One can understand this by looking at electrons through the slave-boson formalism. The physical electron is represented by the operator $f^\dagger_{i\sigma} b_i$, and the Cooper condensate of entangled electrons is then given by $\langle b_i f^\dagger_{i\uparrow} b_j f^\dagger_{j,\downarrow} \rangle \sim \langle b_i b_j \rangle \langle f^\dagger_{i,\uparrow} f^\dagger_{j,\downarrow} \rangle$. This works under the assumption that there is vanishingly small interaction between holons and spinons which is why one can decouple them. Under this assumption, in order to have a Cooper condensate of electrons, we require a spinon-pair condensate as well as a holon condensate.

Chapter 6

Slave-boson mean-field theory with spinon-holon bound states

Kotliar and Liu [4] treated the underdoped Mott insulator as a system of spinons and holon fluctuations. While this captures many interesting and relevant phenomena, one cannot ignore its limitations. As discussed before, in the pseudogap phase of cuprates, we have reason to believe that the area of the Fermi surface, in accordance with Luttinger's theorem, goes as $\sim \delta$ and not $\sim 1+\delta$ (which is expected if the charge carrier is a hole). We have also seen evidence of Fermi arcs that cannot be realized in a free system of spinons and holons. But the dimer model in the $\mathbb{Z}_2$ fractional Fermi liquid regime provides a satisfactory explanation to the appearance of Fermi arcs at low doping densities and gives the correct charge relation that enables Luttinger theorem to hold. It is worth exploring the different phases of matter one expects if the low-energy excitations of the system's Fermi surface are dominated by spinon-holon dimers rather than free spinons and holons.

As shown in equation 4.12, we have a Lagrangian in terms of F, Δ and χ and their complex conjugates. By allowing $\langle\chi\rangle \neq 0$, we access RVB ground states in the system at zero doping.This is seen in the following term of the Lagrangian. $\sim a_3^{\Delta} \sum_{ijkl} \bar{\Delta}_{ij}\Delta_{jk}\bar{\Delta}_{kl}\Delta_{li}$.

Such a system exhibits four possible phases of matter. They are presented in Figure 6.1

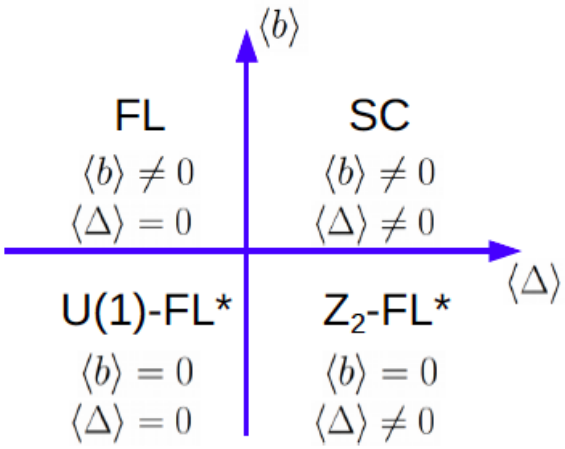

FIGURE 6.1: The schematic phase diagram represents the phases of matter that can exist for the Lagrangian given in equation 4.12 for $\chi \neq 0$. FL and SC denote the Fermi liquid and the superconducting state respectively whereas the states for which $\langle b \rangle = 0$ represent the two kinds of fractional Fermi liquids possible. Figure from 24.

Since $\langle c^\dagger_{k\uparrow} c^\dagger_{-k\downarrow} \rangle \sim \langle bb \rangle \langle f^\dagger_{k\uparrow} f^\dagger_{-k\downarrow} \rangle$, we need both spin-pair condensation and holon condensation for the superconducting state to arise. When spinon-pair condensates do not form, then we have a Fermi liquid state. The state with no holon condensation or pair condensation only has the nonzero spinon hopping term, making it a strange metal. Finally, the phase having only spinon-pair condensation is seen to be the pseudogap phase from the Feynman diagram given in Figure 4.2.

Let us look at the pseudogap phase in particular. From Figure 4.2, we infer the following relation between the electronic and dimeric creation operators. $c_{i\sigma} \sim \sum_j \bar{F}_{ij\sigma} \Delta_{ij} \approx \Delta \sum_j \bar{F}_{ij\sigma}$ for $\langle \Delta \rangle \neq 0$, just as in equation 4.17. Through this relation, one see that the area of the Fermi surface of electrons scales as the number density of dimers, which is equal to the number of holes counted from the half-filling state. This accounts for the discrepancy noted in experiments with respect to Luttinger's relation, and as expected in the pseudogap phase, the area of the Fermi surface scales with δ.

However, it is important to realize that the boundaries between phases given in Figure 6.1 may not lie exactly as depicted. We need to understand the exact form of these boundaries so that we may be able to quantitatively predict the critical temperatures and hole densities for which phase-transitions happen.

6.1 Free energy derivation

So, following a similar methodology as discussed when we studied the free spinon system, we shall explore the exact form of the phase diagram of cuprates if it were

dominated by bound-state excitations. We first attempt to figure out the critical temperatures at which spinon-pair condensates form. This is calculated as a function of hole-density. The action of the system was already worked out in equation 4.9. In order to make it compatible with the results obtained in [4], we redefine the order parameters in a manner similar to 5.12 and rescale the coupling parameter J as was done in 5.17. The action then takes the form:

$$\begin{aligned} S = &\sum_{i,\sigma} \bar{f}_{i\sigma}(\partial_\tau - \mu_F) f_{i\sigma} - J \sum_{i,j,\sigma} \chi_{ij} \bar{f}_{i\sigma} f_{j\sigma} + h.c. - t \sum_{\langle ij \rangle} \bar{f}_{i\sigma} b_i \bar{b}_j f_{j\sigma} \\ &+ \sum_{\langle ij \rangle} J \bar{\Delta}_{ij} (f_{i\uparrow} f_{j\downarrow} - f_{i\downarrow} f_{j\uparrow}) + h.c. + \sum_i \bar{b}_i (\partial_\tau - \mu_F + \mu_B) b_i \\ &+ \frac{2}{3J} \sum_{\langle ij \rangle} (|\chi_{ij}|^2 + |\Delta_{ij}|^2). \end{aligned} \tag{6.1}$$

We first explore the possibility of having a mixed system with both spinon/holon bound states and free spinon/holons. The reason for doing this twofold. One, we construct it in such a way that we can continuously tune the system to move from the pure spinon/holon case to the pure fermionic bound-state case. This allows us to check our results by using the former case as an anchor. Two, it is conceivable that both excitations may be present in a real system and so, it is important that we study the mixed system. The mixed terms are simultaneously introduced in the following manner:

$$-t \sum_{\langle ij \rangle} \bar{f}_{i\sigma} b_i \bar{b}_j f_{j\sigma} = \underbrace{-t(1-\alpha) \sum_{\langle ij \rangle} \bar{f}_{i\sigma} b_i \bar{b}_j f_{j\sigma}}_{\text{H.S. Transf. for spinon/holon excitations}} - \underbrace{t\alpha \sum_{\langle ij \rangle} \bar{f}_{i\sigma} b_i \bar{b}_j f_{j\sigma}}_{\text{H.S. Transf. for dimers}} . \tag{6.2}$$

where α is a tunable parameter that allows us to move from the pure-spinon case ($\alpha = 0$) to the pure dimer case ($\alpha = 1$). Performing the H.S transformations similar to equation (refer), we arrive at the following action:

$$\begin{aligned} S = &\sum_{i,\sigma} \bar{f}_{i\sigma}(\partial_\tau - \mu_F) f_{i\sigma} - \sum_{i,j,\sigma} (J\chi_{ij} + t(1-\alpha)\delta) \bar{f}_{i\sigma} f_{j\sigma} + h.c. \\ &+ \sum_{\langle ij \rangle} J \bar{\Delta}_{ij} (f_{i\uparrow} f_{j\downarrow} - f_{i\downarrow} f_{j\uparrow}) + h.c. + \sum_i \bar{b}_i (\partial_\tau - \mu_F + \mu_B) b_i \\ &+ \frac{2}{3J} \sum_{\langle ij \rangle} (|\chi_{ij}|^2 + |\Delta_{ij}|^2) + + |\Delta_{ij}|^2) + \sum_{i,j} \alpha t \bar{F}_{ij\sigma} F_{ij\sigma} \\ &+ \sum_{ij} \frac{\alpha t_{ij}}{\sqrt{2}} (\bar{F}_{ij\sigma} (f_{i\sigma} b_j + f_{j\sigma} b_i) + h.c.). \end{aligned} \tag{6.3}$$

We now Fourier transform the action. Note that the volume terms $(1/V)$ are absorbed into the momentum sums. First consider the $\sim \bar{F} f b$ terms.

$$
\begin{aligned}
&\sum_{\langle ij\rangle} \frac{\alpha t_{ij}}{\sqrt{2}} \bar{F}_{i,j,\sigma}(f_{i,\sigma} b_j + f_{j\sigma} b_i) + h.c., \\
&= \sum_{i,\eta,\sigma} \frac{\alpha t}{\sqrt{2}} \bar{F}_{i,i+\eta,\sigma}(f_{i\sigma} b_{i+\eta} + f_{i+\eta,\sigma} b_i) + h.c., \qquad \text{with } \eta \in [\pm\hat{e}_x, \pm\hat{e}_y] \\
&= \sum_{\substack{i,\eta,\sigma \\ k,q,p}} \frac{\alpha t}{\sqrt{2}} \bar{F}_{k,\eta,\sigma}(f_{q,\sigma} b_{p+} e^{i(k.r_i - q.r_i - p(r_i+\eta))} + f_{q,\sigma} b_p e^{i(k.r_i - p.r_i - q(r_i+\eta))}) + h.c., \\
&= \sum_{\substack{\eta,\sigma \\ k,q}} \frac{\alpha t}{\sqrt{2}} \bar{F}_{k,\eta,\sigma} f_{q,\sigma} b_{k-q}(e^{-i(k-q).\eta} + e^{-iq.\eta}) + h.c..
\end{aligned}
\tag{6.4}
$$

We assume that all the holons are present in the zero-momentum state. This is an approximation at temperatures higher than the holon-condensation temperature but works well at the temperature scale pertinent to our problem. This entails the following constraint:

$$
b_{k-q} \approx \sqrt{\delta}\,\delta(\vec{k} - \vec{q}). \tag{6.5}
$$

So, we get the following expression.

$$
\sum_{\substack{\eta,\sigma \\ k,q}} \sqrt{\frac{\alpha^2 t^2 \delta}{2}} \bar{F}_{k,\eta,\sigma} f_{q,\sigma}(1 + e^{-iq.\eta}) + h.c. = \sum_{\eta,\sigma,k,q} \sqrt{\frac{\alpha^2 t^2 \delta}{2}} f_{q,\sigma} \bar{\Lambda}_{k,\eta,\sigma} + h.c., \tag{6.6}
$$

where we have defined $\bar{\Lambda}_{k,\eta,\sigma} = \bar{F}_{k,\eta,\sigma}(1 + e^{-iq.\eta})$. Next, we consider:

$$
\sum_{\langle ij\rangle} |\Delta_{ij}|^2 = 2N|\Delta|^2, \tag{6.7}
$$

where we have used the fact that all bonds measure to be Δ and there are $2N$ bonds in total. A similar calculation for χ_{ij} gives

$$
\sum_{\langle ij\rangle} |\chi_{ij}|^2 = 2N|\chi|^2. \tag{6.8}
$$

The next term:

$$\begin{aligned}
&\sum_{\langle ij\rangle}\Delta_{ij}(\bar{f}_{i\uparrow}\bar{f}_{j,\downarrow}-\bar{f}_{i\downarrow}\bar{f}_{j,\uparrow})+h.c.=\sum_{\langle i,i+\eta\rangle}2\Delta_{i,i+\eta}(\bar{f}_i\bar{f}_{i+\eta}-\bar{f}_{i+\eta}\bar{f}_i)+h.c.,\\
&=\sum_{i,k,q,p}\Delta_k\bar{f}_q f_p(e^{i(k.(r_i+x)+q.r_i-p.(r_i+x))}-e^{i(k.(r_i+y)+q.r_i-p.(r_i+y))})+h.c.,\\
&=\sum_{k,q,p}(\Delta_{p-q}\bar{f}_q\bar{f}_p-\Delta_{q-p}\bar{f}_p\bar{f}_q)(e^{i((p-q).x-p.x)}-e^{i((p-q).y-p.y)})+h.c.,\\
&=\sum_k 2\Delta\bar{f}_k\bar{f}_k(2\cos(k_x)-2\cos(k_y)) \qquad \text{using the ansatz } \Delta_{p-q}=\Delta\delta(\vec{p}-\vec{q}).
\end{aligned} \tag{6.9}$$

The next term:

$$\begin{aligned}
\sum_{\langle ij\rangle,\sigma}\alpha t_{ij}\bar{F}_{ij\sigma}F_{ij\sigma}&=\sum_{i,\eta,\sigma}\alpha t_{ij}\bar{F}_{i,i+\eta,\sigma}F_{i,i+\eta,\sigma},\\
&=\sum_{\substack{i,\eta,\sigma\\k,q}}\alpha t\bar{F}_{k,\eta,\sigma}F_{q,\eta,\sigma}e^{i(k.(r_i+\eta)-iq.(r_i+\eta))},\\
&=\sum_{k,\eta,\sigma}\alpha t\bar{F}_{k,\eta,\sigma}F_{k,\eta,\sigma}e^{i(k.\eta-k.\eta)},\\
&=\sum_{k,\eta,\sigma}\alpha t\bar{F}_{k,\eta,\sigma}F_{k,\eta,\sigma}.
\end{aligned} \tag{6.10}$$

The final action is given by:

$$\begin{aligned}
S=&\sum_{k,\sigma}\bar{f}_{k,\sigma}(-i\omega_k+\mu_F+\underbrace{(J\chi+(1-\alpha)t\delta)K_k)}_{\zeta_k}f_{k,\sigma}\\
&+\sum_{\eta,\sigma,k,q}\sqrt{\frac{\alpha^2t^2\delta}{2}}f_{q,\sigma}\bar{\Lambda}_{k,\eta,\sigma}+h.c.\\
&+\sum_k 2J\bar{\Delta}_k\underbrace{(2\cos k_x-2\cos k_y)}_{\Gamma_k}(f_{k,\uparrow}f_{-k,\downarrow})+h.c.\\
&+\frac{4J}{3N}(|\chi|^2+|\Delta|^2)+\sum_k\alpha t\bar{F}_{k,\eta,\sigma}F_{k,\eta,\sigma}.
\end{aligned} \tag{6.11}$$

We can then write the action in Nambu spinor notation as follows:

$$\begin{aligned} S = &\sum_k \begin{pmatrix} \bar{f}_{k\uparrow} & f_{-k\downarrow} \end{pmatrix} \overbrace{\begin{pmatrix} -i\omega_k + \zeta_k & 2J\Delta\Gamma_k \\ 2J\bar{\Delta}\Gamma_k & -i\omega_k - \zeta_k \end{pmatrix}}^{M} \begin{pmatrix} f_{k\uparrow} \\ \bar{f}_{-k\downarrow} \end{pmatrix} \\ &+ \sum_{k,\eta} \begin{pmatrix} \bar{f}_{k\uparrow} & f_{-k\downarrow} \end{pmatrix} \begin{pmatrix} \frac{\alpha t\sqrt{\delta}}{2}\Lambda_{k\eta\uparrow} \\ \frac{\alpha t\sqrt{\delta}}{2}\bar{\Lambda}_{-k\eta\downarrow} \end{pmatrix} \\ &+ \sum_{k,\eta} \begin{pmatrix} \frac{\alpha t\sqrt{\delta}}{2}\bar{\Lambda}_{k\eta\uparrow} & \frac{\alpha t\sqrt{\delta}}{2}\Lambda_{-k\eta\downarrow} \end{pmatrix} \begin{pmatrix} f_{k\uparrow} \\ \bar{f}_{-k\downarrow} \end{pmatrix} + \frac{4J}{3N}(|\chi|^2 + |\Delta|^2) \end{aligned} \tag{6.12}$$

We define the following $f_1 := \begin{pmatrix} f_{k\uparrow} \\ \bar{f}_{-k\downarrow} \end{pmatrix}$ and $\lambda_{k\eta} := \begin{pmatrix} \frac{\alpha t\sqrt{\delta}}{2}\bar{\Lambda}_{k\eta\uparrow} \\ \frac{\alpha t\sqrt{\delta}}{2}\Lambda_{-k\eta\downarrow} \end{pmatrix}$. Consequently, the partition function is written as:

$$Z = \int \mathcal{D}[\bar{f}_{1k}, f_{1k}] e^{-\sum_k \bar{f}_{1k} M f_{1k} + \sum_{k\eta}(\bar{f}_{1k}\lambda_{k\eta} + \bar{\lambda}_{k\eta} f_{1k}) - \alpha t \sum_{k\eta\sigma} \bar{F}_{k\eta\sigma} F_{k\eta\sigma} - 2NJ|\chi|^2 - 2NJ|\Delta|^2}. \tag{6.13}$$

Integrating out the spinon degrees of freedom leaves behind the following F dependent terms:

$$S_{\bar{F},F} = -\sum_{k\eta} \frac{t\delta^2}{2} \begin{pmatrix} \bar{\Lambda}_{k\eta\uparrow} & \Lambda_{-k\eta\downarrow} \end{pmatrix} M^{-1} \begin{pmatrix} \Lambda_{k\eta'\uparrow} \\ \bar{\Lambda}_{-k\eta'\downarrow} \end{pmatrix} + \sum_{k\eta\sigma} \alpha t \bar{F}_{k\eta\sigma} F_{k\eta\sigma}. \tag{6.14}$$

In order to simplify calculations, this is cast into a $4X4$ matrix where the varaibles are the two real-space coordinates and the two Nambu-spinor indices (The matrix is diagonal in momentum space).

$$S_{\bar{F},F} = \sum_{k,\eta,\eta'} \begin{pmatrix} \bar{F}_{k\eta\uparrow} & F_{-k\eta\downarrow} \end{pmatrix} A_{k\eta\eta'} \begin{pmatrix} F_{k\eta'\uparrow} \\ \bar{F}_{-k\eta'\downarrow} \end{pmatrix},$$

$$\text{with } A_{k\eta\eta'} = \begin{pmatrix} \frac{(-i\omega - \zeta_k)((\alpha^2 t^2 \delta/2) g_{k\eta\eta'})}{-\omega^2 - \zeta^2 - 4|\Delta_k|^2} + \alpha t \delta_{\eta\eta'} & -\frac{2\Delta\Gamma_k(\alpha^2 t^2 \delta/2) g_{k\eta\eta'}}{-\omega^2 - \zeta_k^2 - 4|\Delta_k|^2} \\ -\frac{2\bar{\Delta}\Gamma_k(\alpha^2 t^2 \delta/2) g_{k\eta\eta'}}{-\omega^2 - \zeta_k^2 - 4|\Delta_k|^2} & \frac{(-i\omega + \zeta_k)((\alpha^2 t^2 \delta/2) g_{k\eta\eta'})}{-\omega^2 - \zeta_k^2 - 4|\Delta_k|^2} - \alpha t \delta_{\eta,\eta'} \end{pmatrix}. \tag{6.15}$$

where $g_{k\eta\eta'} = (1 + e^{-ik_\eta})(1 + e^{ik_{\eta'}})$. Thus, the total free energy is:

$$S = -\frac{1}{\beta}(\mathrm{Tr}\ln M_k - \mathrm{Tr}\ln A_{k\eta\eta'}) + \frac{4N}{3J}J|\chi|^2 + \frac{4N}{3J}|\Delta|^2, \tag{6.16}$$

where the trace in the first term is over momentum, k, and Nambu space. The trace for the second term is over k, η, η' and Nambu space.

6.2 Zero temperature behaviour of χ and Δ

We minimize the free energy with respect to the parameters $\bar{\Delta}$ and $\bar{\chi}$, we then derive self-consistent equations, which when solved, allows us to extract the behaviour of our system at different temperatures and hole density. In this thesis, we shall focus on the zero temperature results of such a minimization.

$$\frac{\partial S}{\partial \bar{\Delta}} = -\mathrm{Tr}\left(M^{-1}\frac{\partial M}{\partial \bar{\Delta}}\right) - \mathrm{Tr}\left(A^{-1}\frac{\partial A}{\partial \bar{\Delta}}\right) + \frac{4N}{3J}\Delta \stackrel{!}{=} 0. \tag{6.17}$$

Similarly, we minimize the free energy with respect to χ and get:

$$\frac{\partial S}{\partial \bar{\chi}} = -\mathrm{Tr}\left(M^{-1}\frac{\partial M}{\partial \bar{\chi}}\right) - \mathrm{Tr}\left(A^{-1}\frac{\partial A}{\partial \bar{\chi}}\right) + \frac{4N}{3J}\chi \stackrel{!}{=} 0. \tag{6.18}$$

These two equations reduce to the following:

$$1 = \frac{3J}{8N}\int_{-\pi}^{\pi}\frac{d^2k}{4\pi^2}\frac{2\Gamma_k^2}{\xi_k}\tanh\left(\frac{\beta\xi_k}{2}\right), \tag{6.19}$$

$$\chi = -\frac{3J}{8N}\int_{-\pi}^{\pi}\frac{d^2k}{4\pi^2}\left(\frac{2\alpha\delta t + \chi_k + \delta\alpha t K_k/2}{\xi_k}\right)\tanh\left(\frac{\beta\xi_k}{2}\right)K_k. \tag{6.20}$$

To calculate the hole density, we use the same expression derived in the free-spinon system (equation 5.11) for the zero-temperature case. The reason that the same expression works is that the zero-temperature momentum distribution for an electron is independent of the nature of the quasiparticles in the systems, as quasi-particles arise only in finite temperatures. Following a similar argument as in the free spinon calculation (equation5.24), the hole density is given by the following:

$$\delta = \int_{-\pi}^{\pi}\frac{\chi_k}{\sqrt{\chi_k^2 + 4|\Delta|^2\Gamma_k^2}}, \tag{6.21}$$

where the following symbols are used:

$$\begin{aligned}
\Gamma_k =& 2(\cos k_x - \cos k_y),\\
K_k =& 2(\cos k_x + \cos k_y),\\
\chi_k =& \mu_F - (J\chi + t\delta(1-\alpha))K_k,\\
\xi_k =& \big(5\delta^2\alpha^2t^2 + 4\Gamma_k^2|\Delta|^2 + 4\delta\alpha t\chi_k + \chi_k^2 + \frac{1}{2}\delta\alpha t(\delta\alpha t\cos 2k_x + 4(2\delta\alpha t + \chi_k)\cos 2k_y),\\
&+ 4\cos k_y + 4\cos k_x(2\delta\alpha t + \chi_k + \delta\alpha t\cos k_y) + \delta\alpha t\cos 2k_y\big)^{1/2}.
\end{aligned} \tag{6.22}$$

The three self-consistent equations can be solved using a fixed-point iteration. Setting $N, J = 1$ and $t = 10$ [4], we solve these equations separately for different values of alpha at zero temperature. As discussed in the free spinon case, the zero temperature behaviour of the spinon-pairing field is similar to the critical temperature for the formation of the spinon-pair condensate. We expect a similar qualitative trend to hold in this calculation as well. Due to time constraints, we are unable to perform the finite temperature calculations here to compare.

At zero temperature, the three self-consistent equations reduce to:

$$1 = \frac{3J}{8N}\int_{-\pi}^{\pi}\frac{d^2k}{4\pi^2}\frac{2\Gamma_k^2}{\xi_k}, \tag{6.23}$$

$$\chi = -\frac{3J}{8N}\int_{-\pi}^{\pi}\frac{d^2k}{4\pi^2}\left(\frac{2\alpha\delta t + \chi_k + \delta\alpha t K_k/2}{\xi_k}\right)K_k, \tag{6.24}$$

$$\delta = \int_{-\pi}^{\pi}\frac{\chi_k}{\sqrt{\chi_k^2 + 4|\Delta|^2\Gamma_k^2}}. \tag{6.25}$$

We compute the zero-temperature value of Δ and χ as a function of δ. These are plotted for different values of α as shown in figure 6.2.

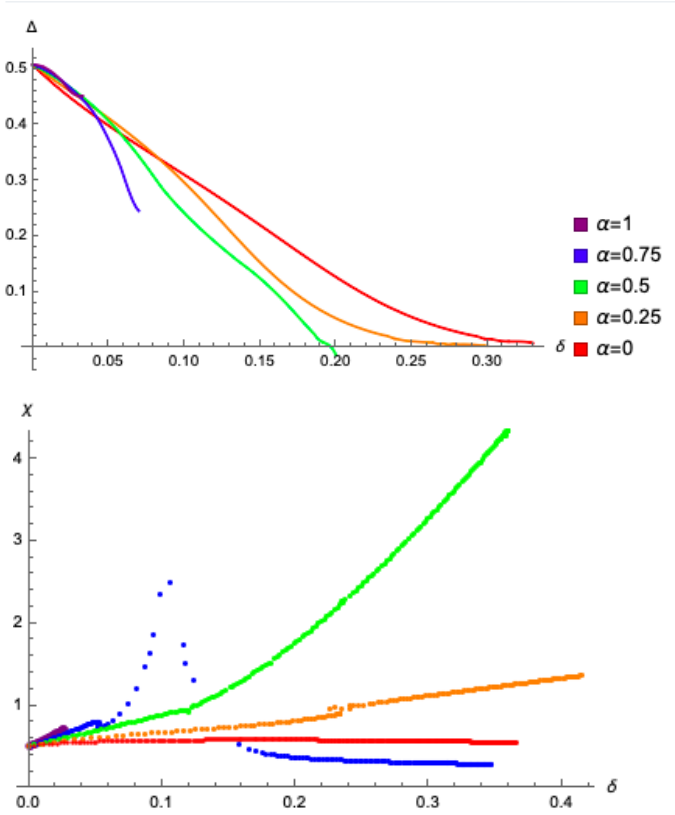

FIGURE 6.2: The two figures represent the Δ vs δ and χ vs δ curves respectively, for different values of α.

Many noteworthy features are observed in Figure 6.2. Firstly, it is noted that the at $\alpha = 0$, both graphs match the free spinon calculation in Figure 5.1. This is encouraging because this tells us that the remainder of the calculation for all other values of alpha are likely to contain the correct constants of proportionality. Second, we see that in the first plot, for $\alpha > 0.5$, that Δ does not smoothly fall to zero. Beyond $\delta \sim 5\%$, the only solution for the self-consistent equations is $\Delta = 0$. This suggests that a system with a strong preference towards forming dimers over free spinons/ holons displays superconductivity or the pseudogap state at extremely low hole doping. Finally, it is also seen that for $\alpha < 0.5$, the form of the Δ curves is qualitatively similar to what is seen in the $\alpha = 0$ case. The only difference is that Δ decays to zero faster for higher values of δ.

Looking at the χ plots, it is immediately obvious that while free spinons and holons give rise to a spinon hopping amplitude that is independent of hole density, the spinon hopping amplitude here rises steeply with the introduction of dimer states in the lattice. Another curious point worth noting is the fact that $\alpha = 1$ does not allow for spinon hopping at higher percentages of hole doping. The reason for this is that hole-doping makes the energy bands in the system more energetic until a point is reached where the lowest energy band of the system is more energetic than the chemical potential. Here, it is energetically favourable for all the electrons to leave the Fermi surface, the holon density is reported to be $\delta \sim 100\%$. This observation is however, not carried forward at $\alpha = 0.75$, where we see that there is a peak in the hopping amplitude beyond which the curve stabilizes at around $\chi \sim 0.3$. However,

an intuitive understanding of these findings is still lacking.

Chapter 7

Conclusion

In this thesis, all our efforts are focused on developing testable predictions of the quantum dimer model which is derived using a slave-boson description of the the t-J model. We derive spin-spin-hole correlations for the $\mathbb{Z}_2$ fractional Fermi liquid in which we assume that low energy excitations of the Fermi surface manifest as dimers. The correlation function is then plotted at different lattice points (Figure 4.5) for all relevant configurations and is compared to a similar plot displayed in Figure 4.6 from experiment [7]. The experiment observes a strong magnetic polaron signal that is seen from the inner electrons being negatively correlated while all other electrons being positively correlated along the diagonals. This is in direct conflict with what was predicted by the $\mathbb{Z}_2$ fractional Fermi liquid. It is seen here that the correlations are strictly negative and the innermost electrons have correlations that are two orders of magnitude larger than the outer electrons. The same calculations are also performed for the Fermi liquid case where a correlation signal that is consistently stronger by an order of magnitude compared to the FL^* case is seen. So, it is clear that for this particular experimental setup, our theory does not match the data observed.

These calculations are repeated for lower temperatures to see if similar qualitative features persist. Figure 4.8 shows that when one goes below $\beta = 11$, the innermost electrons correlate positively with each other while the outer electrons have negative diagonal correlations. The latter is expected for any theory that admits an RVB ground state and hence, is not very surprising. But the correlations of the innermost electrons was unexpected. This is clearly a bold prediction that the quantum dimer model makes, paving the way for future experiments and simulations to test this theory.

We then look at normalized and connected spin-spin-hole correlations for specific configurations as a function of hole density for both the quantum dimer model and the Fermi liquid. These are compared to the experimental data [6] displayed in Figure 4.9. It is seen in Figure 4.10 that the Fermi curve predicted by Wick's theorem through theory matches with the Fermi curve obtained in reference [6] through Monte Carlo simulations. But when we compare the quantum dimer model's predictions to the data points given (Figure 4.10), stark deviations are observed in the low doping regime. One of the key features of Bloch's data is the sign-reversal of the correlation functions observed on the left in Figure 4.9 . Our calculations, on the other hand, predict a strictly negative correlation function for all hole densities.

The same calculations are then repeated at much lower temperatures and shown in Figure 4.11. It is seen that a small crossover is indeed observed within the framework of quantum dimer model itself. While these results are inconclusive at this stage, it seems plausible that the Fermi surface of the $\mathbb{Z}_2$ fractional Fermi liquid is scrambled at the temperatures at which the experiment was performed and that lower temperatures show some distinct features of this phase of matter.

The apparent disparity between the experiments discussed and the predictions made by the quantum dimer model certainly does not entail that we dismiss the quantum dimer model. There are many reasons why the set-up used by Bloch's group may not match the kind of system for which the quantum dimer model is designed to work. It is possible that Bloch's group is operating at a temperature scale that is too high for the quantum dimer model to be relevant. Bloch's group's experiment was set up at $T \sim 1.4J$ where as the spinon-holon bound states have a binding energy $\sim J$. So, it is likely that the bound-state description is not valid at the temperature scale being considered in this experiment. Also, it is often the case that in an optical lattice with ultra-cold atoms, the next-to-nearest hopping of electrons is negligible. However, this hopping term is of primary importance for the pseudogap phase to manifest and the creation of the $\mathbb{Z}_2$ fractional Fermi liquid model. So, if the setup in the experiment does not allow for this phase of matter, the mismatch seen with this model is understandable.

Another aspect of the quantum dimer model we study is the phases that can arise when the underdoped Mott insulator allows for spinon and dimer excitations. Having constructed the t-J model for such a system, we minimize the free energy and derive the the self-consistent equations which, when solved, allow us to predict the different phases that arise at zero temperature. It is encouraging to see that our calculation for the free spinon/holon ($\alpha = 0$ case seen in Figure 6.2) case matches with the expected curves predicted for the free spinon case in Figure 5.1.

It is seen in Figure 6.2 that for a system dominated by electron-hole bound-state excitations, the spinon pairing strength goes discontinuously to zero beyond $\delta \sim 5\%$. This suggests that any sign of superconductivity in such a system will not manifest at larger doping densities. Another curious feature that is seen is that systems which favour bound-state excitations ($\alpha > 0.5$) have spinon-pairing terms that fall to zero discontinuously beyond a critical hole density. Only further investigation will tell us what exactly is happening here.

We also see in Figure 6.2 that the introduction of dimer excitations in a sea of spinon/holon excitations gives rise to a spinon-hopping amplitude that increases with increasing hole density. This is different from what is predicted for the free spinon case where the spinon hopping amplitude shows no strong response to changes in hole density. Another curious feature that was observed for systems with $\alpha > 0.5$ was that the $\chi(\delta)$ curve is nonlinear. This is, however, not seen for the case where there are no free spinon excitations, where we see that no more data points are generated for densities higher than a critical hole density. This suggests the existence of a discontinuous phase transition which leads to a sudden change in particle number,

but it is not clear why this might be happening. Further investigations are required to completely understand all the features that we see in our plots.

7.1 Outlook

There are many interesting problems worth exploring at this stage. We still do not have a clear understanding of why there happens to be a critical hole density beyond which all the order parameters of the spinon-hole bound-state dominated system discontinuously fall to zero. We also wish to solve for the critical temperature required for the spinon-pair condensates to form as a function of hole density. While this is something we can estimate qualitatively from the results we have, a quantitative plot is required in order to make precise predictions. Another problem we could not address in this thesis was that of finding the holon-condensation temperature. Knowledge of this is vital for us to be able to create a complete map of all the phases of the system we expect to see. Finally, it is crucial to understand the relative stability of the bound state excitation with respect to the free spinon/holon excitations in order to be able to make any testable predictions. To do this, we may treat the quantity α as an order parameter of the system and minimize the free energy with respect to it. By simultaneously solving the resulting four self-consistent equations, we may obtain α as a function of hole density. This in turn may give rise to more complex phases that show different behaviours based on the fundamental excitations that permeate the Fermi sea.

Bibliography

[1] J.Bardeen.; L.N.Cooper; J.R.Schrieffer, Microscopic Theory of Superconductivity Physical Review. 106 (1): 162–164 (1957).

[2] Schilling, A.; Cantoni, M.; Guo, J. D.; Ott, H. R. "Superconductivity above 130 K in the Hg–Ba–Ca–Cu–O system". Nature. 363 (6424): 56–58.(1993)

[3] Louis Taillefer. Scattering and pairing in cuprate superconductors. Annual Review of Condensed Matter Physics, 1, Mar 2010.

[4] G. Kotliar and J. Liu, Superexchange mechanism and d- wave superconductivity," Phys. Rev. B 38, 5142 (1988)

[5] M. Plat'e, J. Mottershead, I. Elfimov, D. Peets, R. Liang, D. Bonn, W. Hardy, S. Chiuzbaian, M. Falub, M. Shi, L. Patthey, and A. Damascelli, Fermi Surface and Quasiparticle Excitations of Overdoped $Tl_2Ba_2CuO_{6+\delta}$," Phys. Rev. Lett. 95, 077001 (2005).

[6] J. Koepsell, D. Bourgund, P. Sompet, et al. arXiv:2009.04440v1 [cond-mat.quant-gas]

[7] J.Koepsell, J.Vijayan, P.Sompet et al. Imaging magnetic polarons in the doped Fermi–Hubbard model. Nature 572, 358–362 (2019).

[8] M.Punk, A.Allais, and S.Sachdev. Quantum dimer model for the pseudogap metal. Proceedings of the National Academy of Sciences, 112(31):9552–9557, (2015).

[9] P.Coleman, New approach to the mixed-valence problem, Phys. Rev. B. The American Physical Society. 29 (6): 3035–3044. (1984).

[10] H.-B. Yang, J. D. Rameau, Z.-H. Pan, et al. Reconstructed Fermi surface of underdoped $Bi_2Sr_2CaCu_2O_{8+\delta}$ cuprate superconductors. Phys. Rev. Lett., 107:047003, (2011).

[11] S.I.Mirzaei, D.Stricker, J.N.Hancock, et al. Spectroscopic evidence for Fermi liquid-like energy and temperature dependence of the relaxation rate in the pseudogap phase of the cuprates. Proceedings of the National Academy of Sciences of the United States of America, 110(15):5774– 5778,(2013)

[12] T.C. Ribeiro and X.G.Wen. New mean-field theory of the $tt't''J$ model applied to high-Tc superconductors. Phys. Rev. Lett., 95:057001, (2005).

[13] Tai-Kai Ng. Spinon-holon binding in tJ model. Phys. Rev. B, 71:172509, (2005).

[14] S. I. Mirzaei, D. Stricker, J. N. Hancock, C. Berthod, A. Georges, E. van Heumen, M. K. Chan, X. Zhao, Y. Li, M. Greven, N. Barisic, and D. van der Marel, Spectroscopic evidence for Fermi liquid-like energy and temperature dependence of the relaxation rate in the pseudogap phase of the cuprates," Proc. Nat. Acad. Sci. 110, 5774 (2013)

[15] M. K. Chan, M. J. Veit, C. J. Dorow, Y. Ge, Y. Li, W. Tabis, Y. Tang, X. Zhao, N. Barisic, and M. Greven, In-Plane Magnetoresistance Obeys Kohler's Rule in the Pseudogap Phase of Cuprate Superconductors," Phys. Rev. Lett. 113, 177005 (2014).

[16] C.Chen, T.Yuan, Y.Qi, Z.Y.Meng. Fermi arcs and pseudogap in a lattice model of a doped orthogonal metal, arXiv:2007.05543v4 [cond-mat.str-el]

[17] A. Damascelli, Z. Hussain, and Z.-X. Shen, Angleresolved photoemission studies of the cuprate superconductors," Rev. Mod. Phys. 75, 473 (2003).

[18] K. M. Shen, F. Ronning, D. H. Lu, F. Baumberger, N. J. C. Ingle, W. S. Lee, W. Meevasana, Y. Kohsaka, M. Azuma, M. Takano, H. Takagi, and Z.-X. Shen, Nodal Quasiparticles and Antinodal Charge Ordering in $Ca_{2-x}Na_xCuO_2Cl_2$," Science 307, 901 (2005).

[19] H.-B. Yang, J. D. Rameau, Z.-H. Pan, G. D. Gu, P. D. Johnson, H. Claus, D. G. Hinks, and T. E. Kidd, Reconstructed Fermi Surface of Underdoped $Bi_2Sr_2CaCu_2O_{8+\delta}$ Cuprate Superconductors," Phys. Rev. Lett. 107, 047003 (2011).

[20] Cooper, Leon. "Bound Electron Pairs in a Degenerate Fermi Gas". Physical Review. 104 (4): 1189–1190. Bibcode:1956PhRv..104.1189C (1956)

[21] C. Castellani, C. Di Castro, D. Feinberg, and J. Ranninger, Phys. Rev. Lett. 43, 1957 (1979).

[22] X. G. Wen and R. Kan, Phys. Rev. B 37, 595 (1988).

[23] Fukuyama,On Magnetic Properties of High Tc Oxides, H.,1992, Prog. Theor. Phys. Suppl. 108, 287

[24] J. Brunkert, M. Punk, A slave boson description of pseudogap metals in t-J models arXiv:2002.04041v1 [cond-mat.str-el]

[25] P.Lee, N.Nagaosa, X.Wen, Doping a Mott Insulator: Physics of High Temperature Superconductivity, arXiv:cond-mat/0410445v1 [cond-mat.str-el]

[26] S.Alexandrov, J.T.Devreese, Advances in Polaron Physics (Springer, 2010).

[27] Mark S. Hybertsen, E. B. Stechel, M. Schluter, and D. R. Jennison, Renormalization from density-functional theory to strong-coupling models for electronic states in Cu-O materials, Phys. Rev. B 41, 11068 (1990)

[28] Patrick A. Lee and Naoto Nagaosa, Gauge theory of the normal state of high-Tc superconductors, Phys. Rev. B 46, 5621 (1992)

[29] G. Baskaran, Z. Zou, P.W. Anderson, Solid State Commun. 63, 973 (1987)

[30] A.Altland, B.Simons, Condensed Matter Field Theory. Cambridge University Press. (2006)

[31] K. Tanaka,et al. (2003), Effects of next-nearest-neighbor hopping t' on the electronic structure of cuprates , arXiv:cond-mat/0312575v1 [cond-mat.supr-con]

[32] A. Auerbach, Interacting Electrons and Quantum Magnetism; Springer, New York, NY (1994)

[33] C.Gross, I. Bloch, Quantum simulations with ultracold atoms in optical lattices. Science 357, 995–1001 (2017).

[34] A.Mazurenko, et al. A cold-atom Fermi–Hubbard antiferromagnet. Nature 545, 462–466 (2017).

[35] P.T.Brown, et al. Bad metallic transport in a cold atom Fermi–Hubbard system. Science 363, 379–382 (2019).

[36] M.A.Nichols, et al. Spin transport in a Mott insulator of ultracold fermions. Science 363, 383–387 (2019).

[37] G.Salomon, et al. Direct observation of incommensurate magnetism in Hubbard chains. Nature 565, 56–60 (2019); correction 566, E5 (2019).

[38] D.Rokhsar and S. Kivelson, Superconductivity and the quantum hard-core dimer gas. Phys. Rev. Lett., 61:2376–2379, (1988).

Declaration of Authorship

I, Shashank Anand, declare that this thesis titled, “Effective theories of the underdoped 2D Mott Insulator” and the work presented in it are my own. Any contributions from others have been duly acknowledged and the usage of existing results in literature have been duly cited.

.....
München, June 29th, 2021,
Shashank Anand